Francois, G., Cooper, J. E., & Weaver, P. M. (2016). Impact of the Wing Sweep Angle and Rib Orientation on Wing Structural Response for Un-Tapered Wings. In 57th AIAA/ASCE/AHS/ASC Structures, Structural Dynamics, and Materials Conference. [AIAA 2016-0472] American Institute of Aeronautics and Astronautics Inc, AIAA. 10.2514/6.2016-0472

Impact of the Wing Sweep Angle and Rib Orientation on Wing Structural Response for Un-Tapered Wings

G. Francois[1], J. E. Cooper[2] and P. M. Weaver[3]
Department of Aerospace Engineering, University of Bristol, Bristol, BS8 1TR, UK.

In this paper, the impact of varying the sweep angle of the spar and the rib orientation on wing structural deformation is investigated and related to a beam model. 3D Finite-Element wing wind tunnel models with varying wing sweep angle and rib orientation are considered. The wing models tip displacement and tip twist under static tip loads and aerodynamic loading are considered as well as the wing's natural frequencies, aeroelastic instability speed and maximum root bending moment during a gust encounter. A framework to characterise Euler-Bernoulli beam properties on wings with geometric coupling is then developed and validated to relate the stiffness and bend/twist coupling parameter to the full FE models.

I. Introduction

The airline industry is expected to see a growth of 5% per annum for the next two decades[1]. In order to support such growth a number of challenges need to be tackled among which the industry's dependency on fossil fuel is one of the biggest. Aircraft designers and manufacturers are therefore looking at ways to reduce aircraft fuel consumption.

The science of aeroelasticity focuses on the deformation and response of structure under aerodynamic, inertia and elastic forces[2]. Applied to wing design, aeroelasticity can control the wing shape during cruise flight, control the wing response to gust encounters and also prevent the occurrence of flutter and divergence. Thus the control of aeroelastic properties of a wing could offer some weight and fuel savings, and this is known as aeroelastic tailoring[3].

The control of aeroelastic properties is achieved through the control and coupling of bending and torsion deflections. Such control has been principally achieved through the use of composite materials where the stiffness tailoring is achieved through the control of the fibre orientation[4–9]. More recently research work has focused on the use of the wing structure shape and arrangement to improve aeroelastic properties[10–23]. Such work clearly highlighted the potential offered by shape and topology optimisation for aeroelastic tailoring. However this is achieved through the use of optimisation methods with coupled Finite Element (FE) and Computation Fluid Dynamics (CFD) where the physical understanding as to why a certain solution is better than another is often hard to understand. Additionally, certain concepts generated can be too complex to translate into a manufactural design leaving engineers perplexed as to what to do next. Finally, such optimisation methods suffer from the discrepancy between the tools needed and the decisions variables used in the design process. Indeed, such methods require high fidelity FE models - which are often generated at the detail design phase - but uses decision variables such as spar and rib positions which are set in the preliminary design phase.

Therefore, there is a clear need to further develop the understanding between wing shape and wing deformation by varying the structural arrangement of a standard wing structure composed of spars, ribs and covers both through modelling and experiment. In this effort, Harmin et *al*[24] showed the impact of varying the rib/spar orientation on the wing deformation while Francois et *al*[25,26] attempted to illustrate such impact through a series of experiments using 3D printed wings. Additionally, there is a need to translate this understanding into simple tools that designers can use in the early design phase to make a better judgement as to how the structural members should be arranged.

Beam models have been extensively used to describe the capacity of composite materials to influence the bending and torsional deflections. Such models also characterise a wing structure deformation by using three cross-sectional stiffness parameter around a reference axis. According to Weisshaar[5], the bending moment (M) and torque (T) can relate to the bending (w'') and twist (θ') curvature along the reference axis using

[1] PhD Research Student
[2] Royal Academy of Engineering Airbus Sir George White Professor of Aerospace Engineering, AFAIAA
[3] Professor in Lightweight Structures

$$\begin{bmatrix} M \\ T \end{bmatrix} = \begin{bmatrix} EI & -K \\ -K & GJ \end{bmatrix} \begin{Bmatrix} w'' \\ \theta' \end{Bmatrix} \tag{1}$$

where *EI* and *GJ* are the bending and torsional stiffness parameter and *K* is the bend/twist coupling parameter. When dealing with composite materials, K is a function of the material properties.

The interest and use of the beam model can be understood when considering the numerous advantages that the beam model offers to designers. First, such a model is easy to implement while providing a way to include the bend/twist coupling possibilities of a composite material and for this reason is often used in the preliminary design stage. Additionally, the use of a single term to characterise the bend/twist coupling capability of a stacking-sequence, K, offers designers with an easy comparison metric. Considering such advantages, there is a need to develop a frame-work to enable the identification of beam properties that can characterise geometric bend/twist coupling.

In this paper, the impact of the wing sweep angle and the rib orientation on the wing static and dynamic structural response for aeroelastic performances is characterised numerically. In addition, the characterisation of the wing's bend/twist coupling due to the wing sweep angle and the rib orientation is related to a simple structural beam model.

II. Concept Explored and Wing Dimensions

A. Concept Explored

In this paper, the wing sweep angle and the rib orientation are changed to assess their impact on the wing deformation as shown by Figure 1.

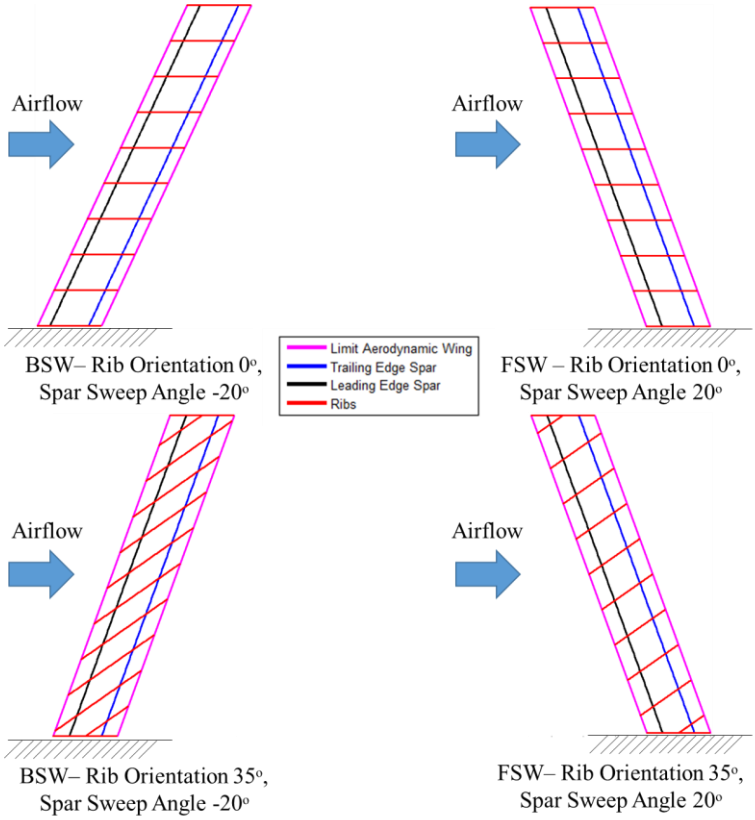

Figure 1. Illustration of the Different Structural Arrangement Considered in this Paper on Backward Swept Wing (BSW) and Forward Swept Wing (FSW).

B. Wing Model

The different wind tunnel wing designs considered in this paper are all un-tapered and of similar general dimensions with a span of 500mm and a chord of 100mm. The skin and spar thickness are 2mm and 4mm

respectively. The wing's internal structure was made of 8 ribs, 2 spars and a root and tip ribs. The leading and trailing edge spar were placed at 25% and 75% of the wing chord, respectively. So as to avoid an increase in the skin panel size a change in rib orientation created a half rib at each end of the wing. Finally the wing box is of a constant thickness to chord ratio of 9.5%. The constant thickness to chord ratio was approximated by converting a NACA0012 profiled wing section into an equivalent rectangular wing box. This was done assuming thin-wall beam theory and considering the second moment of area contribution of the different structural members using

$$h = \sqrt{\frac{\sum h_i^2}{n}} \tag{2}$$

where, h is the equivalent rectangular wing box height, h_i is the actual height of element i on the NACA profile wing box and n is the number of element considered. In this case only the two spars were considered. The wing sweep angle was varied from -30° to 30° with 5° increments. Rib orientation between -45° to 45° with 5° increments were considered initially. Such rib orientation design space was reduced as the sweep angle increased to prevent the connection of the first/last rib with the root/tip rib. The wing geometry dimensions, sweep angle and rib orientation sign conventions are summarised in Figure 2. A rib orientation of 0° means that the ribs are placed stream wise irrespective of the sweep angle and the rib thickness is of 4mm. For a given sweep angle the variation of the rib orientation from the 0° orientation implies an increase/decrease in rib length and the addition of a half rib at the tip and root thus to maintain the wing mass constant, the rib thickness was varied as the rib orientation changes.

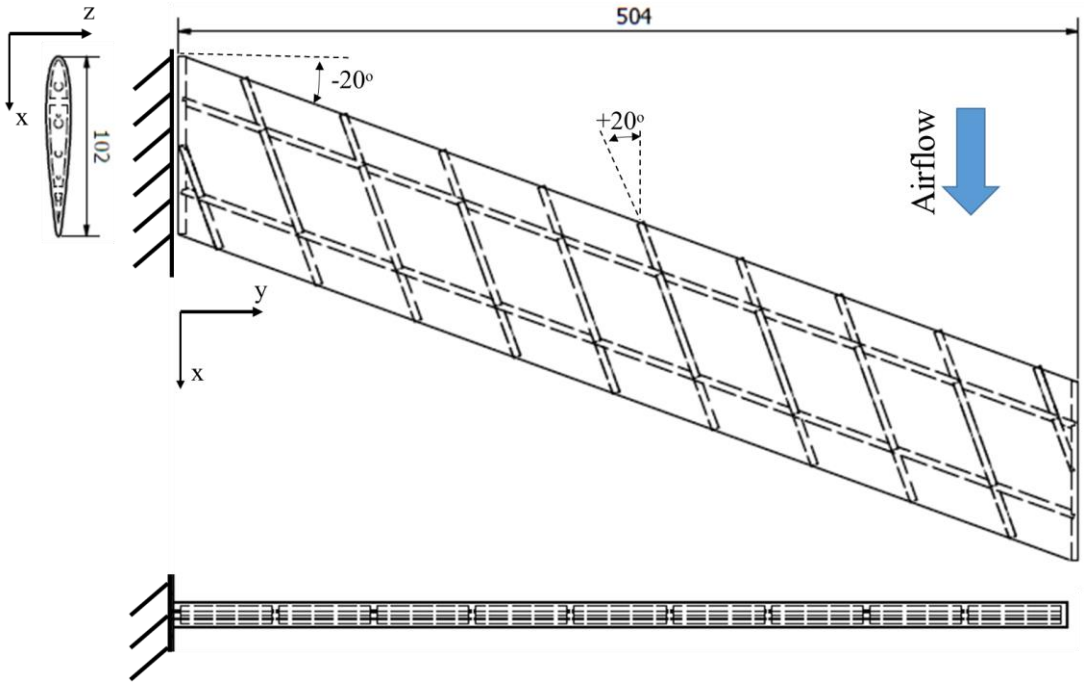

Figure 2. Example of Wing External Dimensions in mm and Sweep Angle and Rib Orientation Conventions.

The wing was assumed to be made in a solidified polyamide material - a material used in previous experiments[25,26]- with a Young's modulus of 1,650.0MPa, a Poisson's ratio of 0.4 and a density of 1.15g/cm^3. The material was assumed to be isotropic and homogenous.

III. Finite-Element Modelling

In this section, the impact of the sweep angle and the rib orientation on the wing deformation is illustrated through the use of 3D Finite Element (FE) model using 2D shell elements. The average tip displacement is calculated by averaging the displacement at the leading and trailing edge. Nose up twist is shown by a positive twist value.

A. Finite Element Modelling

The different wing models considered in this paper were analysed using Finite Element analysis. A MATLAB routine which created a MSC.PATRAN session file for the different wing design considered was used. This file was then run in MSC.PATRAN and contained all the necessary actions to create an FE model such as the creation of the surfaces, meshing of the surfaces, node equivalence and check of the element geometries as well as the creation of element properties and boundary conditions to be used in the different analyses. IsoMesh and Paver meshing algorithms were used to mesh the wing models. The models used 2D shell elements (CQUAD4 and CTRIA3). Element geometry was checked to avoid highly skewed elements. The model mesh contained over 50,000 structural elements and 900 aerodynamic panels for the aeroelastic calculations.

B. Static Analysis

Figure 3-6 show the variation in tip displacement and tip twist as the wing sweep angle and the rib orientation are changed when the wing is subjected to a tip load of 487g applied at the mid-chord. When the ribs are stream wise, the tip displacement and tip twist increases as the wing sweep angle increases. The tip displacement increases by a similar amount and sign for both forward and negative sweep. It is interesting to note that this effect can be interpreted as the spars behaving more like ribs – reducing their contribution to the wing bending stiffness. On the other hand, the tip twist increases proportionally to the sweep angle and with the same sign as the sweep angle. The variation of the rib orientation can also modify the tip displacement and tip twist; however, the impact due to the sweep angle is greater than the one due to the rib orientation.

In the case of an unswept wing, the tip displacement initially reduces as the rib orientation changes due to the addition of the half rib at the root and tip. Then the tip displacement increases until a rib orientation of 25° past which the tip displacement decreases as the ribs start stiffening the wing. The variation in tip twist due to the rib orientation is a cubic curve with two turning points with maximum tip twist values achieved at a high rib orientation. The rib orientation can control the sign of the tip twist.

In the case of a forward swept wing, increasing the rib orientation by a negative value reduces the tip displacement. In the case of a positive increase in rib orientation, the tip displacement first slightly reduces and then slightly increases after a rib orientation of 25°. This is similar but inverse behaviour to that of a backward swept wing.

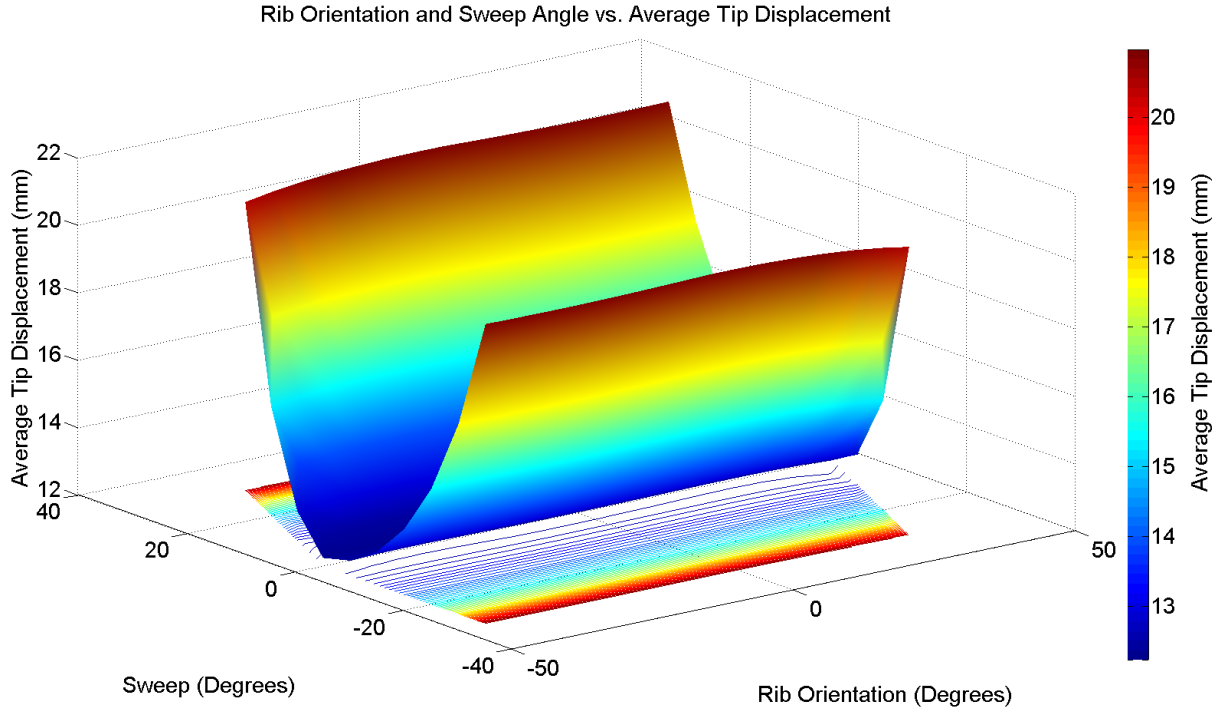

Figure 3. Average Tip Displacement for various Wings with different Rib Orientation and Wing Sweep Angle under Static Load Applied at the Tip Mid-Chord.

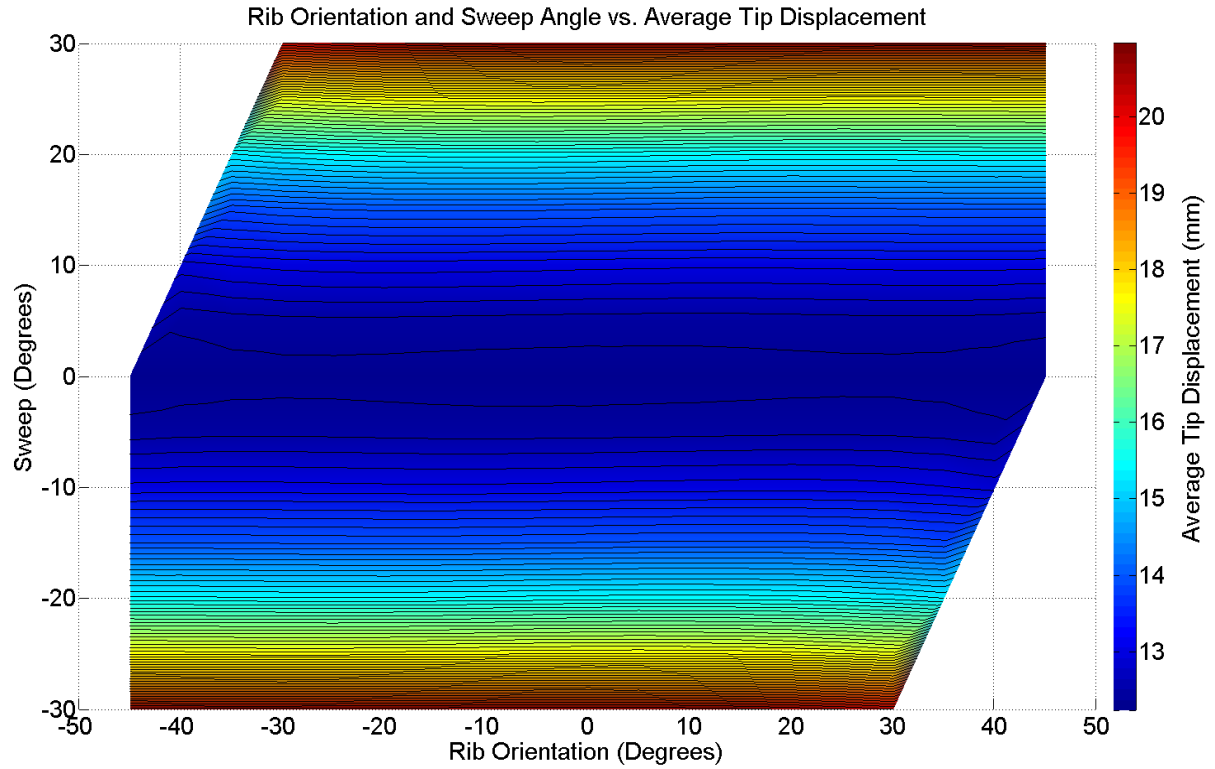

Figure 4. 2D Representation of the Impact of Varying the Wing Sweep Angle and the Rib Orientation on the Average Tip Displacement under Static Load Applied at the Tip Mid-Chord.

Figure 5. Average Tip Twist for various Wings with different Rib Orientation and Wing Sweep Angle under Static Load Applied at the Tip Mid-Chord.

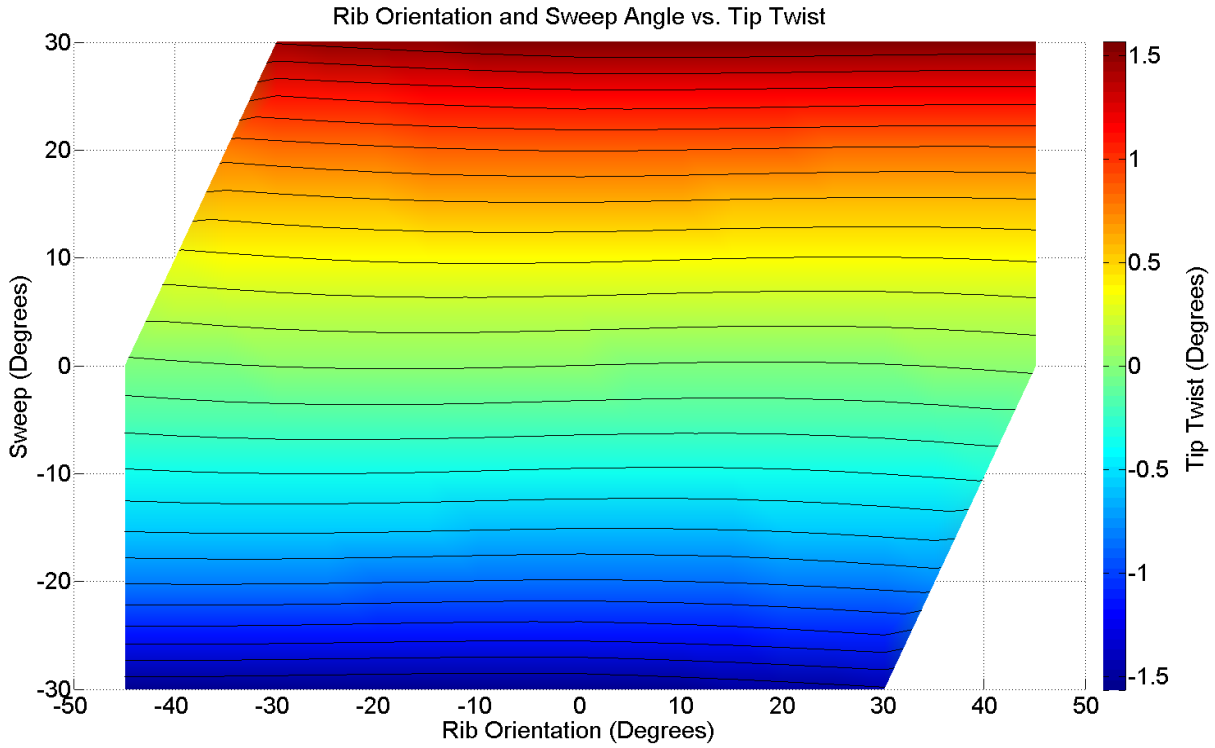

Figure 6. 2D Representation of the Impact of Varying the Wing Sweep Angle and the Rib Orientation on the Tip Twist under Static Load Applied at the Tip Mid-Chord.

As shown by Figure 3-6, the variation of the wing sweep angle and the rib orientation modify the bend/twist coupling of the wing. One way to represent such variation is to plot the flexural axis of the wing which is the line joining the sectional flexural centres where the flexural centre is the point on the wing section where the application of a shear load results in no rotation of that particular section with respect to the root[27,28]. Section flexural centres are found by applying a unit load at distinct points on a wing's section. Figure 7 shows the location of the flexural axis for five different wings: (1) sweep angle of -20° and rib orientation of 0°; (2) sweep angle of 20° and rib orientation of 0°; and (3-5) sweep angle of 0° and rib orientation of -45°, 0° and 45°. This information allows the reader to understand the creation and extent of the geometric bend/twist coupling created by varying the rib orientation and the wing sweep angle. For example, in the case of an un-swept wing, the placement of the ribs at a negative angle displaces the flexural axis towards the leading edge. Hence a vertical load applied at the tip mid-chord results in a nose down twist. A nose-up twist would be created in the case of a negative rib orientation.

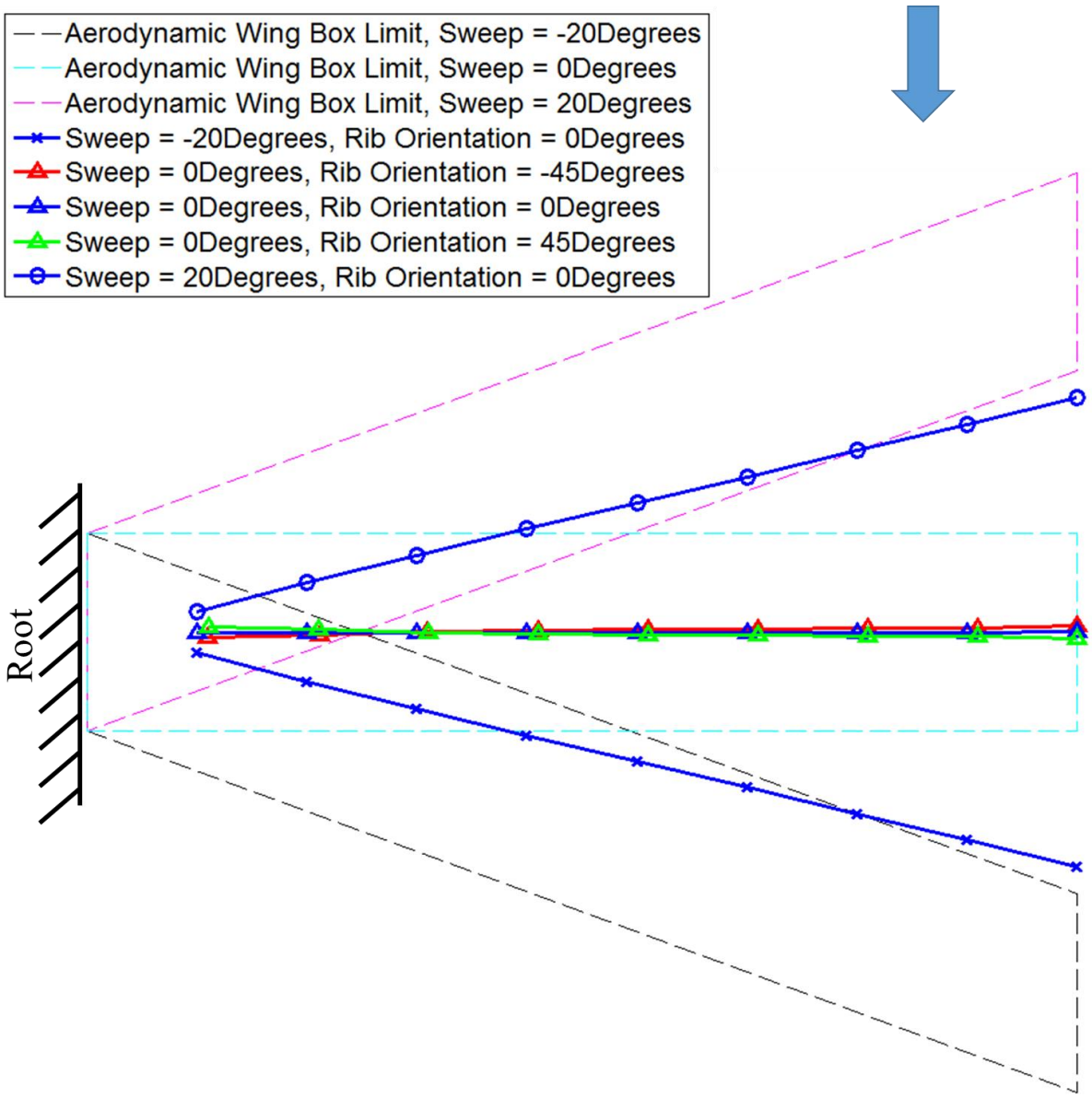

Figure 7. Flexural Axis Plot for Various Wings with different Rib Orientation and Wing Sweep Angle.

C. Static Aeroelastic Analysis

Figure 8-11 show the variation of tip displacement and twist as the sweep angle and the rib orientation change when the wing is subject to aerodynamic loading at a speed of 35m/s and an angle of attack of 5° at a temperature of 25°C. The wing root was fully fixed and a symmetric aerodynamic loading at the root was assumed to mimic wing tunnel wall reflection[29]. As shown previously, the variation in sweep angle and rib orientation can change the wing tip displacement and twist.

For forward-swept wings, increasing the sweep angle leads to an increase in tip displacement and tip twist. Indeed as the wing is swept further forward any increase in bending also leads to an increase in tip twist which increases the angle of attack at the tip and therefore increases the loading.

In the case of the backward-swept wing, increasing the sweep angle from 0° to -10° reduces the tip displacement and nose-up tip twist. After a sweep angle of -10°, increasing the sweep angle increases the tip displacement and increases the nose-down tip twist.

When considering the rib orientation, it is clear that increasing the rib orientation can reduce the tip displacement especially if the rib orientation is negative. This effect can be explained by the coupling created by the rib

orientation and sweep angle and the addition of a half-rib in the first half of the chord at the root – location of the maximum aerodynamic loading - when the rib orientations are negative. The largest impact of rib orientation is on forward swept wings.

Varying the rib orientation at a certain sweep angle changes the tip twist cubic curve. In the unswept case, the curve has two distinct turning points. The curve tends to a convex/concave curve for a wing sweep angle of -30°/30°.

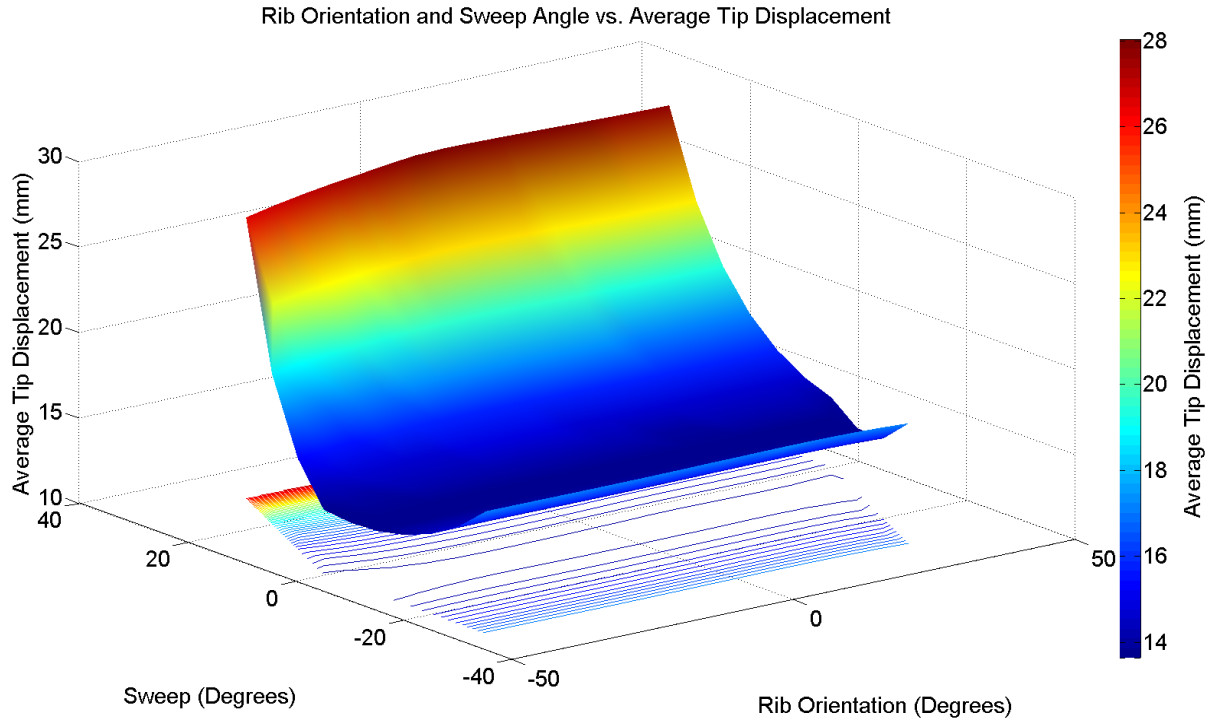

Figure 8. Average Tip Displacement for various Wings with different Rib Orientation and Wing Sweep Angle under Aerodynamic Loading at Speed of 35m/s and an Angle of Attack of 5°.

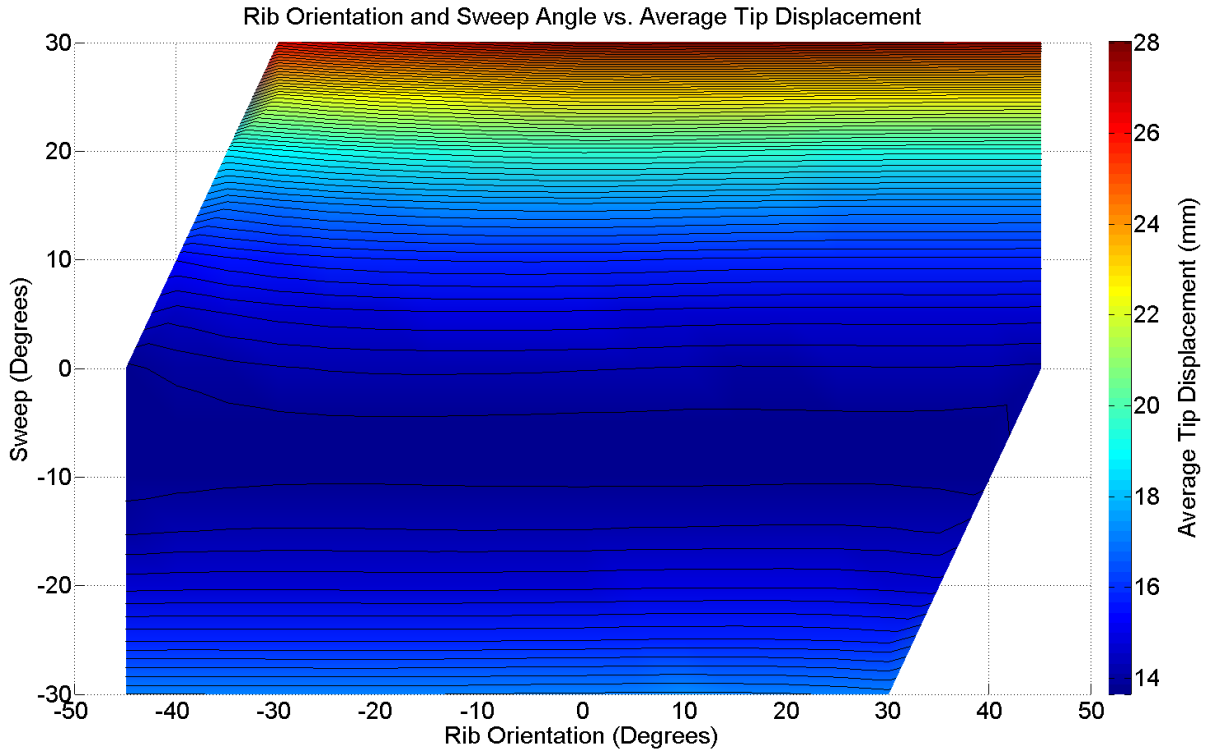

Figure 9. 2D Representation of the Impact of Varying the Wing Sweep Angle and the Rib Orientation on the Average Tip Displacement under Aerodynamic Loading at Speed of 35m/s and an Angle of Attack of 5°.

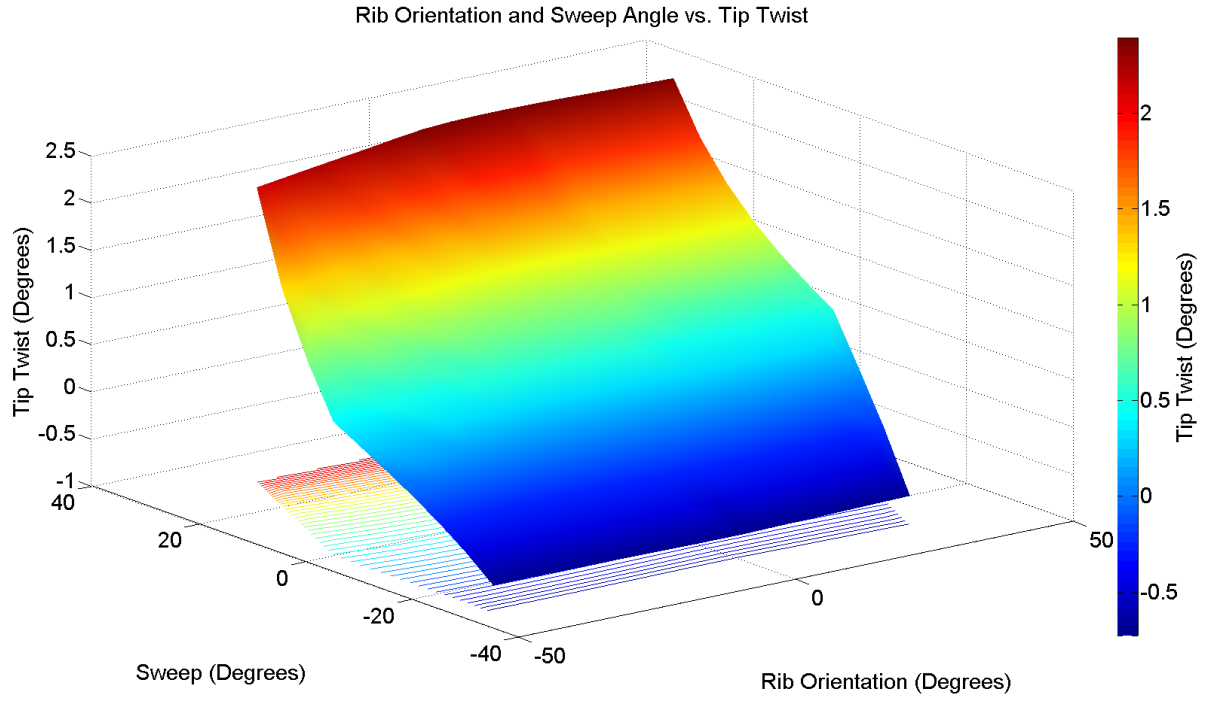

Figure 10. Tip Twist for various Wings with different Rib Orientation and Wing Sweep Angle under Aerodynamic Loading at Speed of 35m/s and an Angle of Attack of 5°.

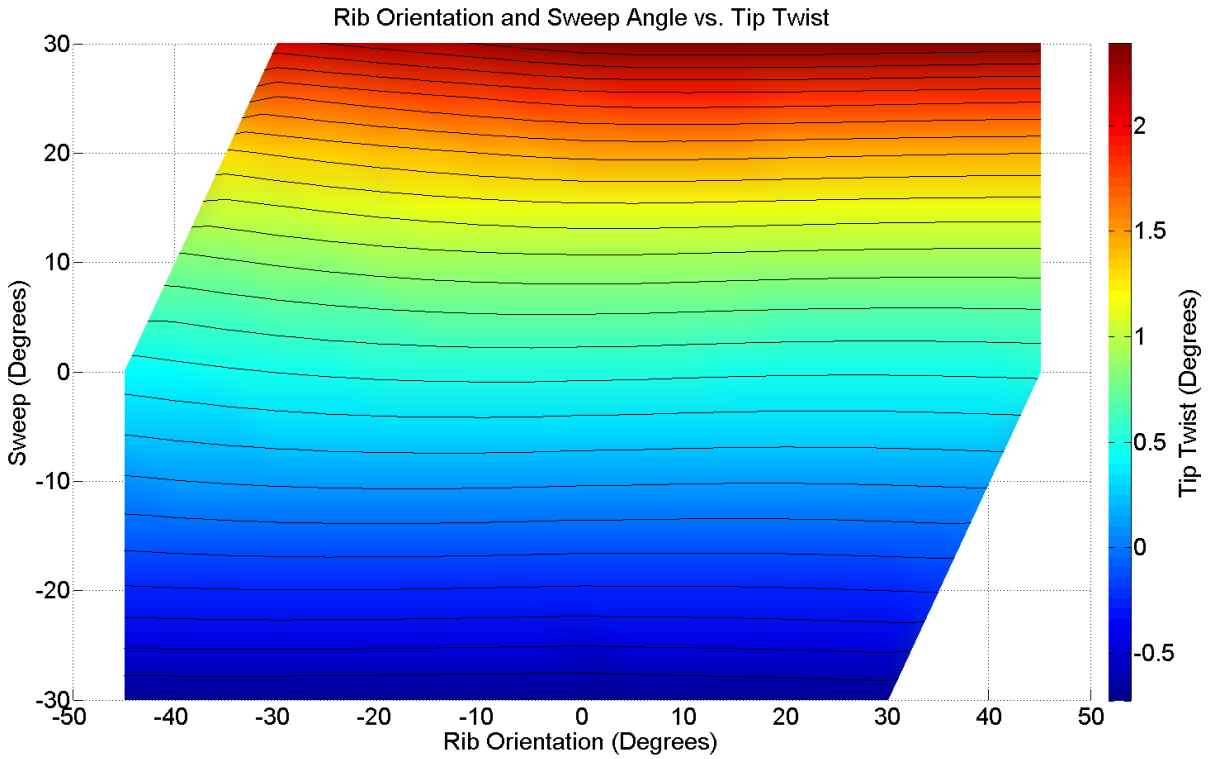

Figure 11. 2D Representation of the Impact of Varying the Wing Sweep Angle and the Rib Orientation on the Tip Twist under Aerodynamic Loading at Speed of 35m/s and an Angle of Attack of 5°.

D. Natural Frequency Analysis

Figure 12 and Figure 13 show the variation of the first four natural frequencies as the wing sweep angle and the rib orientation are changed. Clearly, the rib orientation and the wing sweep angle have an impact on the natural frequencies of a wing.

In the case of an un-swept wing, the variation of the natural frequencies due to the variation of the rib orientation is found to be symmetrical about the 0° rib orientation. The first four modes are: first bending, second bending, forward/aft and first torsion. The change in rib orientation does not change the mode order but varies the modes natural frequencies. For mode 1, 2 and 3 the natural frequencies slightly reduce in values when the rib orientation changes from 0° to ±30° and then increase above a rib orientation of ±35°. Mode 4 natural frequency strictly increases with a variation in rib orientation from the 0°.

When the wing sweep angle is varied - while the rib orientation is at 0° - the natural frequencies of the first three modes are found to decrease as the sweep angle magnitude increase. It should be noted that the change in wing sweep angle triggers a change in mode order past a value of 10°. When the sweep angle is above a magnitude of 10°, the first four modes are first bending, forward/aft, second bending and first torsion instead of first bending, second bending, forward/aft and first torsion.

For a given wing sweep angle, the variation in rib orientation results in a change in the natural frequencies for the first four modes which is not symmetric about the 0° orientation. However a symmetry in the natural frequencies values exist when considering wings with opposite sweep angle and opposite rib orientation. For example, the wing with a sweep angle of 20° and a rib orientation of 45° has similar natural frequencies values compared to the wing with a sweep angle of -20° and a rib orientation of -45°. Indeed both these wings have similar angles between the ribs and spars - similar structural arrangement.

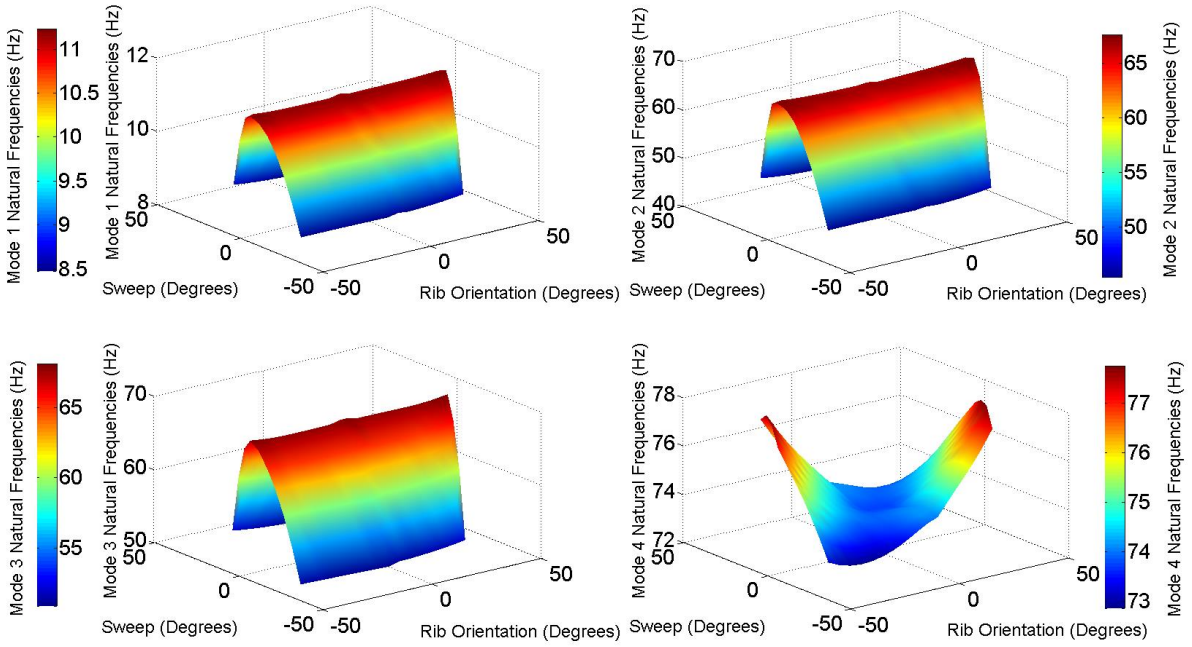

Figure 12. First Four Natural Frequencies for various Wings with different Rib Orientation and Wing Sweep Angle.

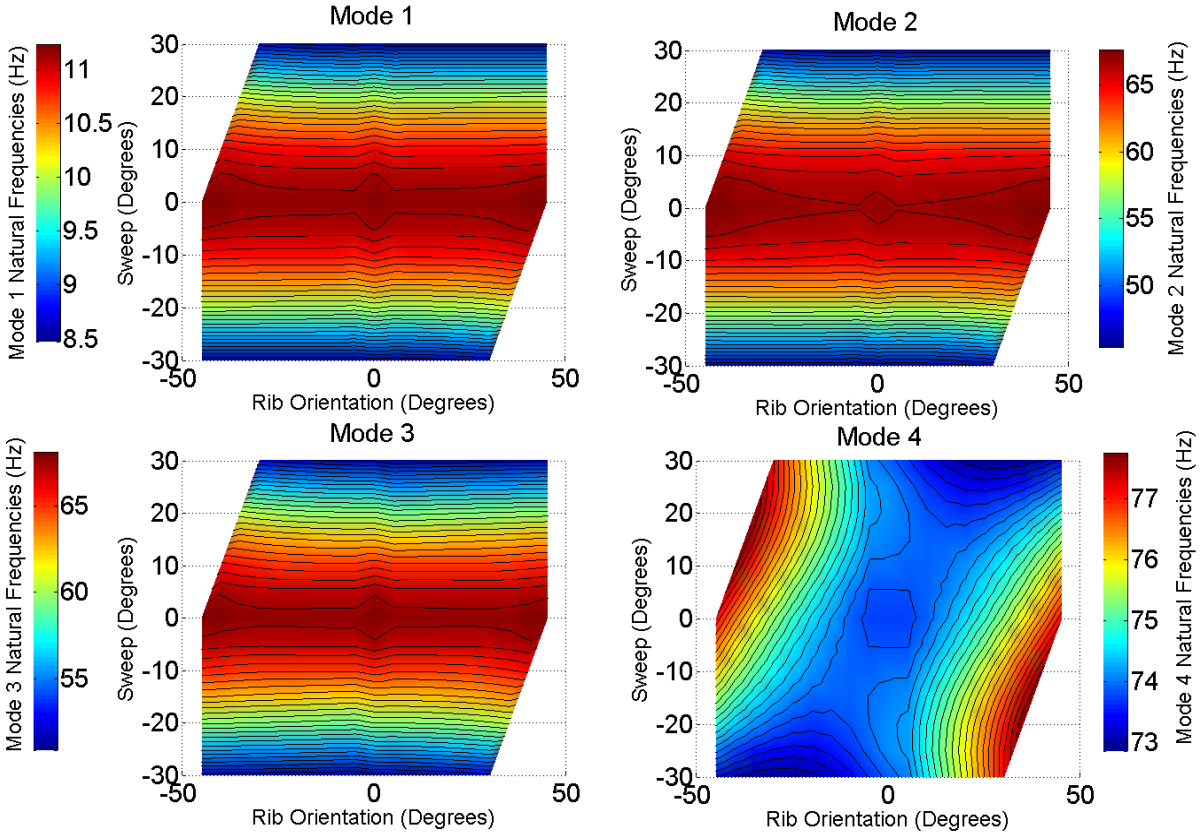

Figure 13. 2D Representation of the Impact of Varying the Wing Sweep Angle and the Rib Orientation on the First Four Natural Frequencies.

E. First Aeroelastic Instability Speed Analysis

The aeroelastic instability speed analysis was performed using MSC.NASTRAN PKNL analysis (SOL 145)[29,30]. The analysis was performed at an altitude of 0m and at 25°C with Mach number ranging from 0.01 to 0.5. A symmetry at the root was assumed to consider the reflection from the wind tunnel wall[29]. The inclusion of 0.5% of structural damping prevented the triggering of soft flutter modes[2,29]. Figure 14 and Figure 15 show the variation of the first aeroelastic instability speed as the wing sweep angle and the rib orientation are changed. The variation of the wing sweep angle has clearly a larger impact than the rib orientation.

When considering backward swept wings, increasing the sweep angle leads to a reduction in the first aeroelastic instability speed by up to 12.8%. The first aeroelastic instability is always due a coalescing of the first and second wing mode and is a flutter instability.

Changing the rib orientation on un-swept and backward swept wings can lead to an increase of the first aeroelastic instability speed by up to 6.1%. The first aeroelastic instability is always flutter due to the coalescence of the first and second wing modes. The rib orientation leading to the minimum flutter speed for a given wing speed is always negative with a value increasing as the sweep angle increases. For example, the un-swept wings achieve lowest flutter speed with ribs oriented at -5°, while a wing with a sweep of -30° does so at a rib orientation of -20°.

When considering forward swept wings the variation of the first aeroelastic instability speed with the wing sweep angle can be split in three regions: (1) sweep angle at 5°, (2) sweep angle between 10° to 20° and (3) sweep angle superior to 20°. When the forward sweep angle is greater than 20°, the first aeroelastic instability speed is always due to divergence of the first bending mode and increases as the sweep angle reduces. For a given sweep angle, only two divergence speeds were found for all rib orientations considered. For a wing sweep of 25°, placing the ribs at an orientation between -30° and -15° increases the divergence speed by 5.3% compared to the other rib orientation available. The rib orientation for the divergence speed step increment moves towards the positive rib orientation region as the sweep angle increases.

When the wing sweep angle is between 10° and 20° the wings were found to flutter with mode four damping values becoming negative by a small amount (0.5-1.5%). In some cases a "hump" flutter was observed although structural damping of 0.5% had been added to the structure. Increasing the sweep angle was found to increase the flutter speed by up to 19.9%. For a given sweep angle, the lowest flutter speed was found for wings with positive rib orientation varying between 10° to 20° depending on the sweep angle.

When the wing sweep angle is placed at 5°, the aeroelastic instability behaviour of the wing is highly dependent on the rib orientation. For a rib orientation between -40° to -20° and between 0° to 45° the wing flutter due to the instability of mode four similarly to wings with sweep angle between 10° to 20°. When the rib orientation is between -15° to -5°, the wing undergoes first bending mode divergence. This change in aeroelastic instability behaviour implies that the control of the rib orientation can lead to an 88.0% increase in the first aeroelastic instability speed for a wing with a sweep angle of 5°.

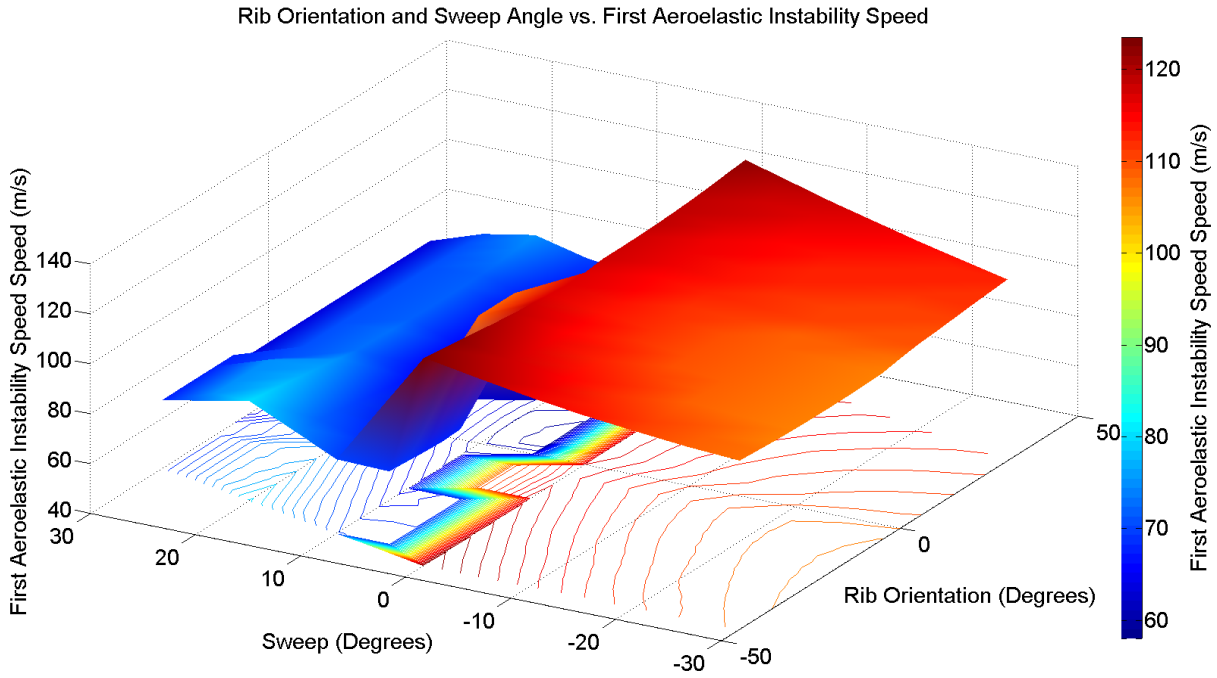

Figure 14. First Aeroelastic Instability Speed for various Wings with different Rib Orientation and Wing Sweep Angle.

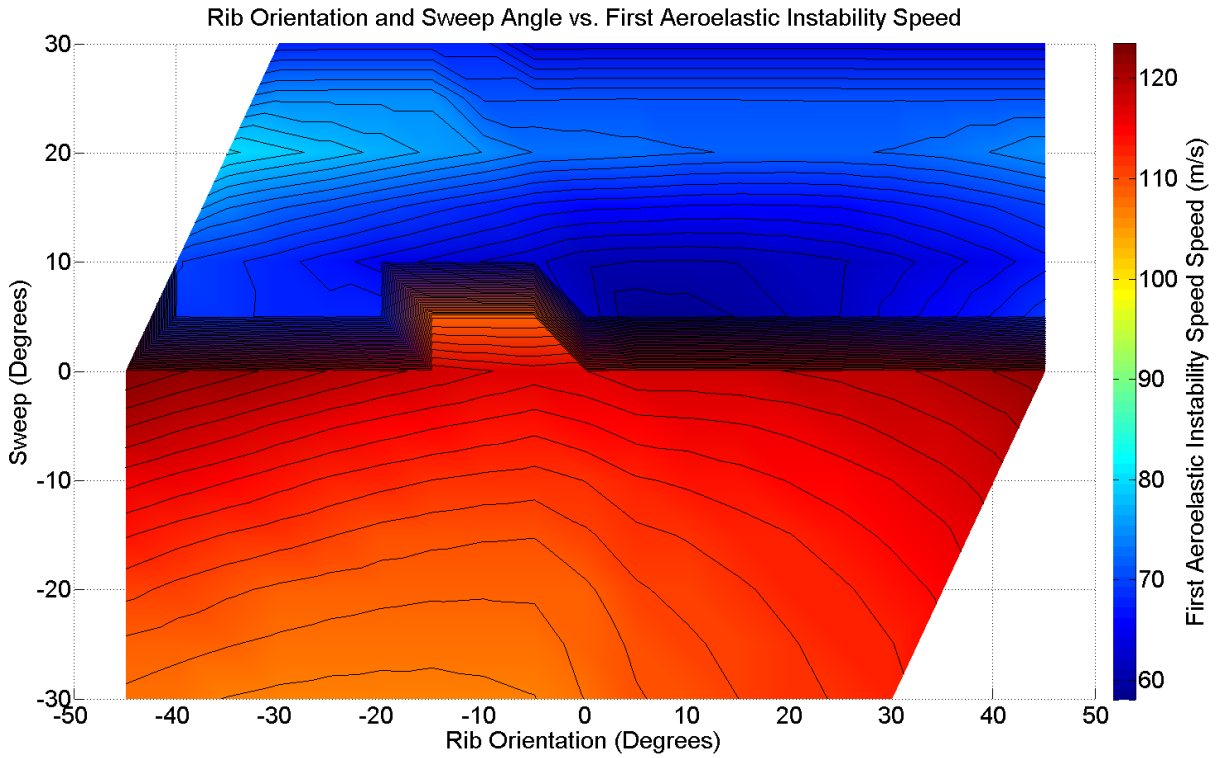

Figure 15. 2D Representation of the Impact of Varying the Wing Sweep Angle and the Rib Orientation on the First Aeroelastic Instability Speed.

F. Gust Load Analysis

In this paper, a single '1-Cosine' gust event was considered using MSC.NASTRAN SOL 146 for which the time domain gust velocity is expressed using

$$w_g(t) = \frac{w_{g0}}{2}\left(1 - \cos\frac{2V\pi}{L_g}t\right) \tag{3}$$

with t the analysis time variable, w_g , 0.5m/s, the peak gust velocity and the gust length L_g [2]. The gust analysis was performed at an altitude of 0m and at a speed of 35m/s at 25°C. Only one gust length of 25 times the mean chord of wing was used[31]. A symmetry at the root was assumed to consider the reflection from the wind tunnel wall[29]. A value of 0.5% of structural damping was used in this analysis. The wing root is assumed to be fully fixed through a Multiple Point Constraint (MPC).The wing root bending moment was assessed by considering the bending moment created on the node slaving all the nodes at the root.

Figure 16 and Figure 17 show the variation of the maximum root bending moment encountered during a gust event as the sweep angle and the rib orientation are changed. The variation of the sweep angle has clearly a larger impact on the root bending moment then the rib orientation. It is interesting to notice that when the rib orientation is at 0° the maximum root bending moment is experienced by a wing with a forward sweep angle of 15°. Increasing or decreasing the sweep angle away from this value reduces the root bending moment. The lowest root bending moment was experienced by the wings with a sweep angle of -30°. The reduction in bending moment as the sweep angle decreases from 15° to -30° can be related to the reduction in tip displacement and twist under aerodynamic loading shown by Figure 8-11. On the other hand, the reduction in root bending moment observed when the sweep angle is increased from 15° to 30° is harder to understand.

The impact of the rib orientation is dependent on the wing sweep angle. However a change in rib orientation by 5° from the stream wise position always leads to a reduction in root bending moment. This can be explained by the introduction of a half rib at the root which stiffen the wing.

Additionally, in all the wing sweep angle considered placing the ribs to a negative orientation leads to a reduction in root bending moment compared to the stream wise rib orientation case and is due to the bend/twist coupling due to the sweep angle and the rib orientation.

Figure 16. Maximum Bending Root Generated Moment during a Gust Encounter for various Wings with different Rib Orientation and Wing Sweep Angle under Aerodynamic Loading at Speed of 35m/s.

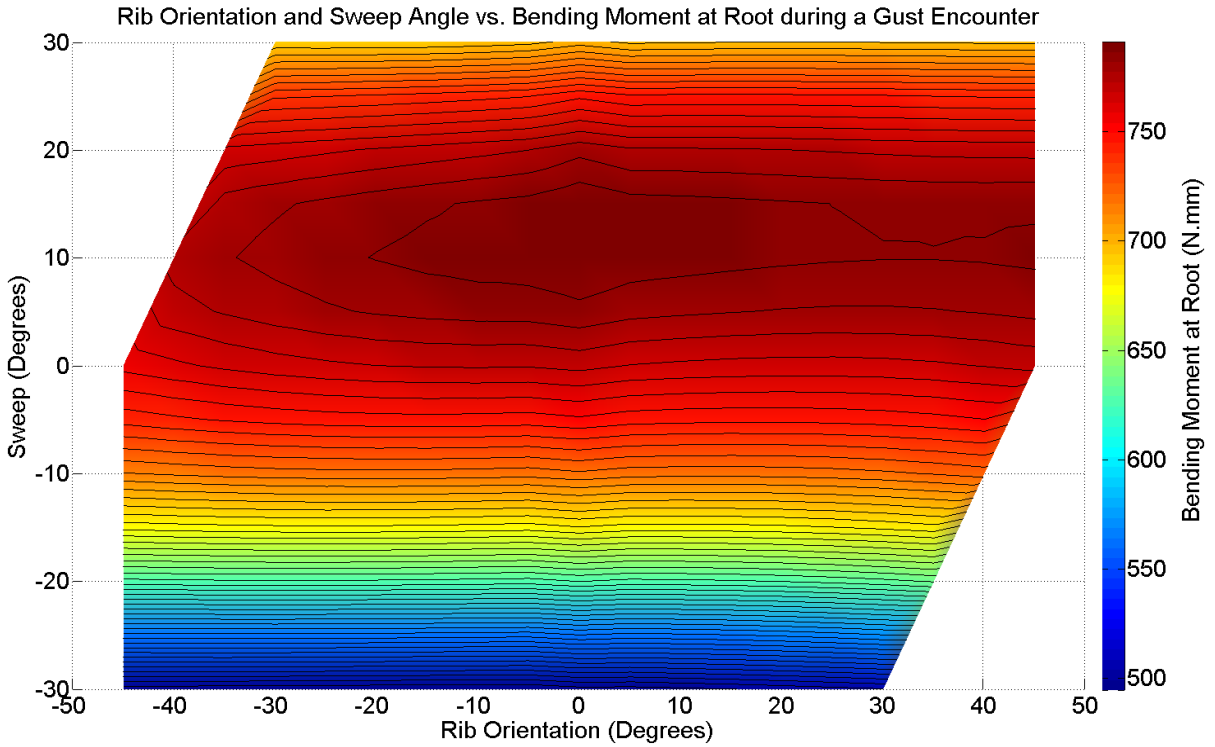

Figure 17. 2D Representation of the Impact of Varying the Wing Sweep Angle and the Rib Orientation on the Maximum Root Bending Moment Generated during a Gust Event.

IV. Beam Model Properties Identification Framework

As can be seen in Figure 7, the use of the flexural axis to quantify the amount of bend/twist coupling existing in a particular wing concept is complex to implement and also requires a high level of interpretation. There is a need to use a simpler comparison metric such as the one found in an Euler-Bernoulli beam model, where according to Weisshaar[5], the bending (w'') and twist (θ') curvature of a beam section is related to the sectional bending moment (M) and torque (T) along the reference axis using

$$\begin{bmatrix} M \\ T \end{bmatrix} = \begin{bmatrix} EI & -K \\ -K & GJ \end{bmatrix} \begin{Bmatrix} w'' \\ \theta' \end{Bmatrix} \tag{4}$$

where EI and GJ are the bending and torsional stiffness parameter and K is the bend/twist coupling parameter. Assuming that the bending moment is due to the application of a tip load and the torque is applied at the tip of a beam of length L $(y = L)$, Equation 4 can be rearranged to relate the bending deflection (w) and twist (θ) with the bending moment and torque using

$$\begin{bmatrix} Py^2(3L - y)/6 \\ Ty^2/2 \end{bmatrix} = \begin{bmatrix} EI & -K \\ -K & GJ \end{bmatrix} \begin{Bmatrix} w \\ \theta y \end{Bmatrix} \tag{5}$$

When dealing with composite materials, K is a function of the material properties and can be determined analytically. In the case of geometric bend/twist coupling, as shown by Figure 3-6, no such formula exists. Hence to determine the beam properties of a wing with geometric bend/twist coupling, 3D FE model outputs can be curve-fitted to match the beam model using the following framework.

3D FE wing models were placed under 2 different load cases: (1) a tip load of 10N at the wing tip flexural centre and (2) a torque of 2,000N.mm at the wing tip flexural centre. Assuming that the application of a tip load at the wing tip flexural centre deforms the wing in pure bending, Equation 5 for load case 1 can be rewritten as

$$Py^2(3L - y)/6 = EIw \tag{6}$$

In the second load case, a torque is applied which produces both bending and twist deflection. However, in the beam equation the loads are considered un-coupled, thus Equation 5 becomes

$$\begin{bmatrix} 0 \\ Ty^2/2 \end{bmatrix} = \begin{bmatrix} EI & -K \\ -K & GJ \end{bmatrix} \begin{Bmatrix} w \\ \theta y \end{Bmatrix} \tag{7}$$

From equations 6 and 7, EI, GJ and K at a section of the wing can be found. Using this framework (summarised by Figure 18), EI, GJ and K values at different sections along the wing can be found as shown by Figure 19, Figure 20 and Figure 21 for an un-swept wing.

As the rib orientation is increased both the tip section bending and torsional stiffness increase. The increase is symmetric by the 0^o orientation. This is due to the ribs stiffening the wing as they behave more like spars. It should be noticed that the shape of the bending stiffness curve is similar to the tip displacement curve for an un-swept wing when the load is applied at the tip as shown by Figure 3. It is interesting to note that a 100mm from the root the bending and torsional stiffness values are higher than the one found at subsequent sections. This effect is due to the root constraint and the assumption that a tip load applied at the wing tip flexural centre places the wing in pure bending.

Varying the rib orientation clearly controls the sign of the bend/twist coupling parameter. Opposite rib orientations create opposite bend/twist coupling parameter values. The variation of the tip section bend/twist coupling parameter with the rib orientation is a cubic curve with two turning points. However the curve is almost linear at 100mm from the root and above 200mm the curve is a cubic curve with two turning points similar to the tip twist curve for an un-swept wing when the load is applied at the tip as shown by Figure 5. The change in shape

along the length of the wing is due to the root effect. Further error is introduced away from the wing tip section by the assumption that a tip load applied at the wing tip flexural centre places the wing in pure bending.

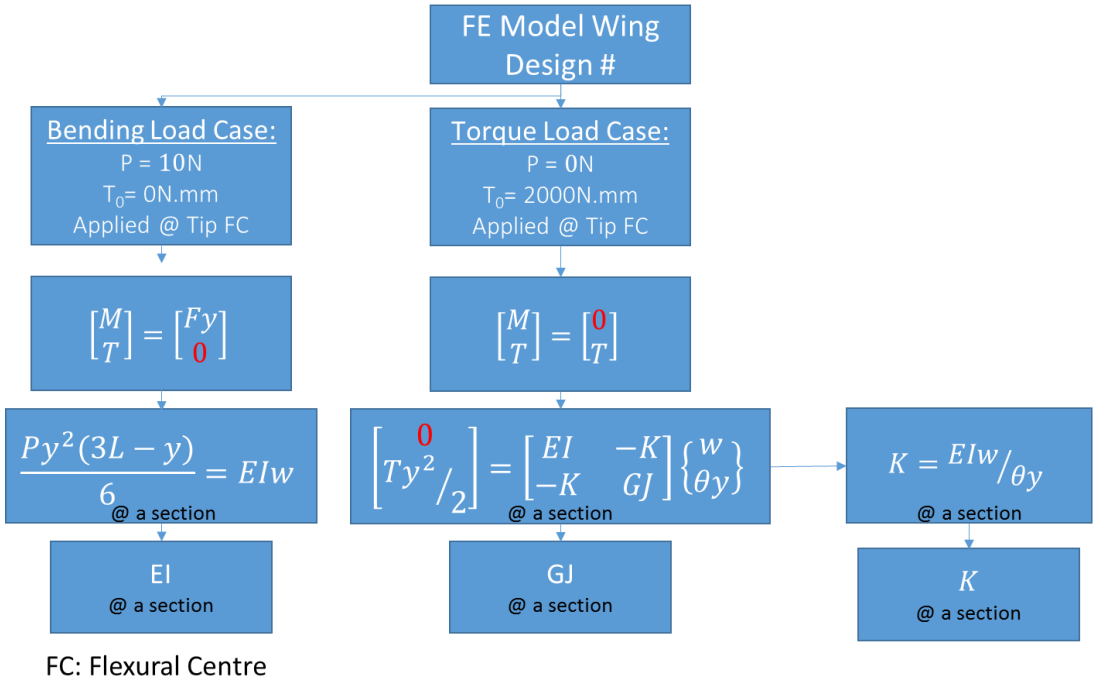

Figure 18. Framework used to Capture Beam Properties of a Wing with Geometric Bend/Twist Coupling.

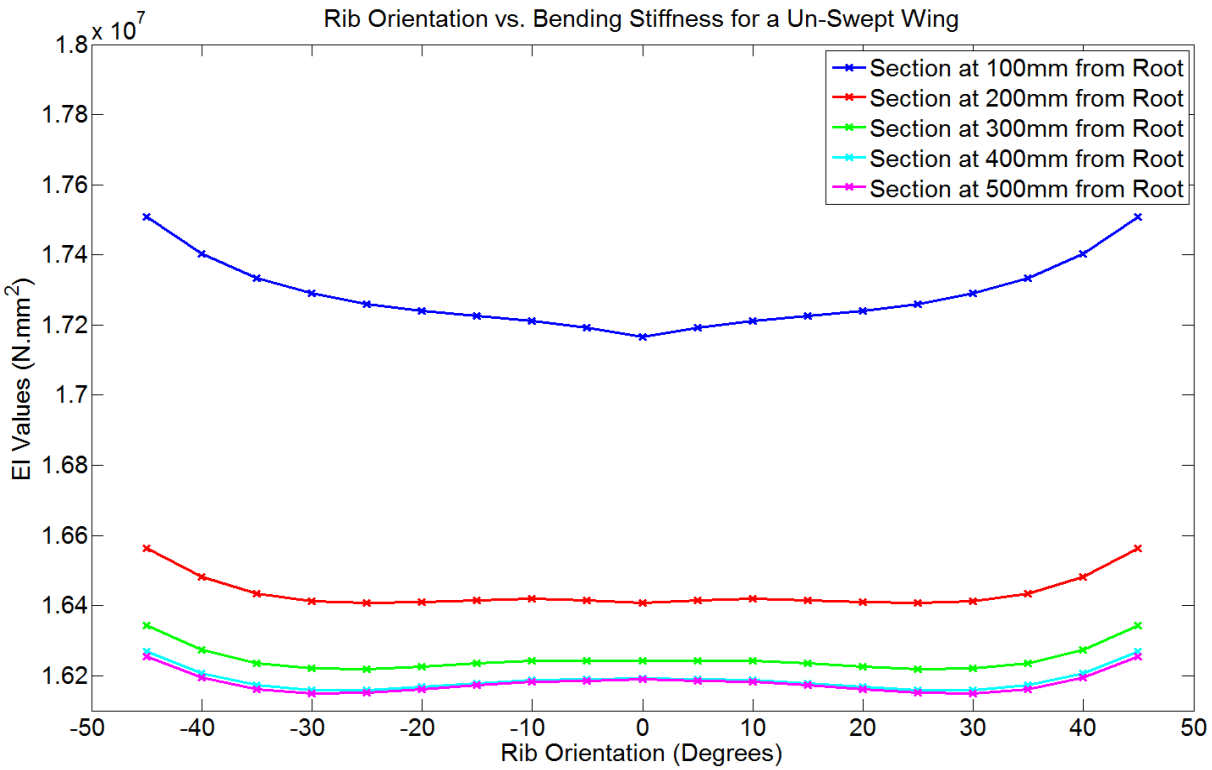

Figure 19. Bending Stiffness Value (EI) Obtained at different Sections along the Wing for an Un-Swept Wing with varying Rib Orientation.

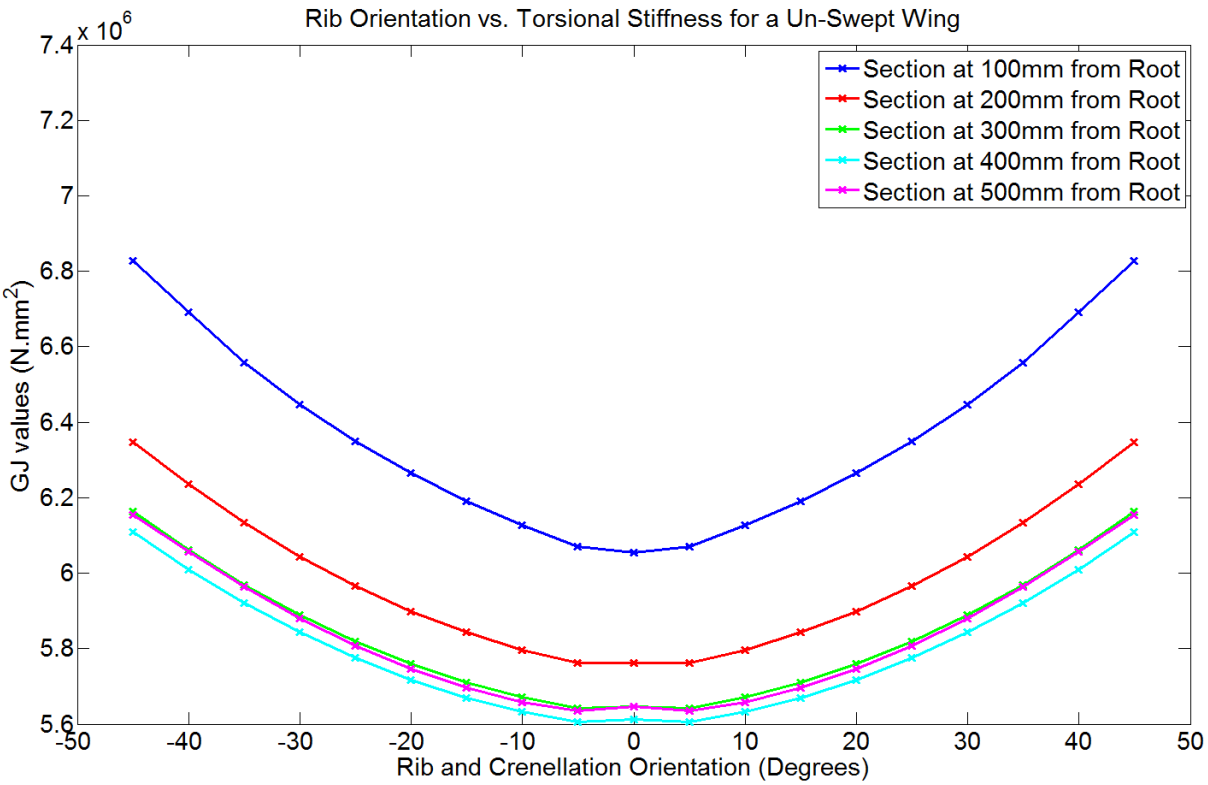

Figure 20. Torsional Stiffness Value (GJ) Obtained at Different Sections along the Wing for an Un-Swept Wing with varying Rib Orientation.

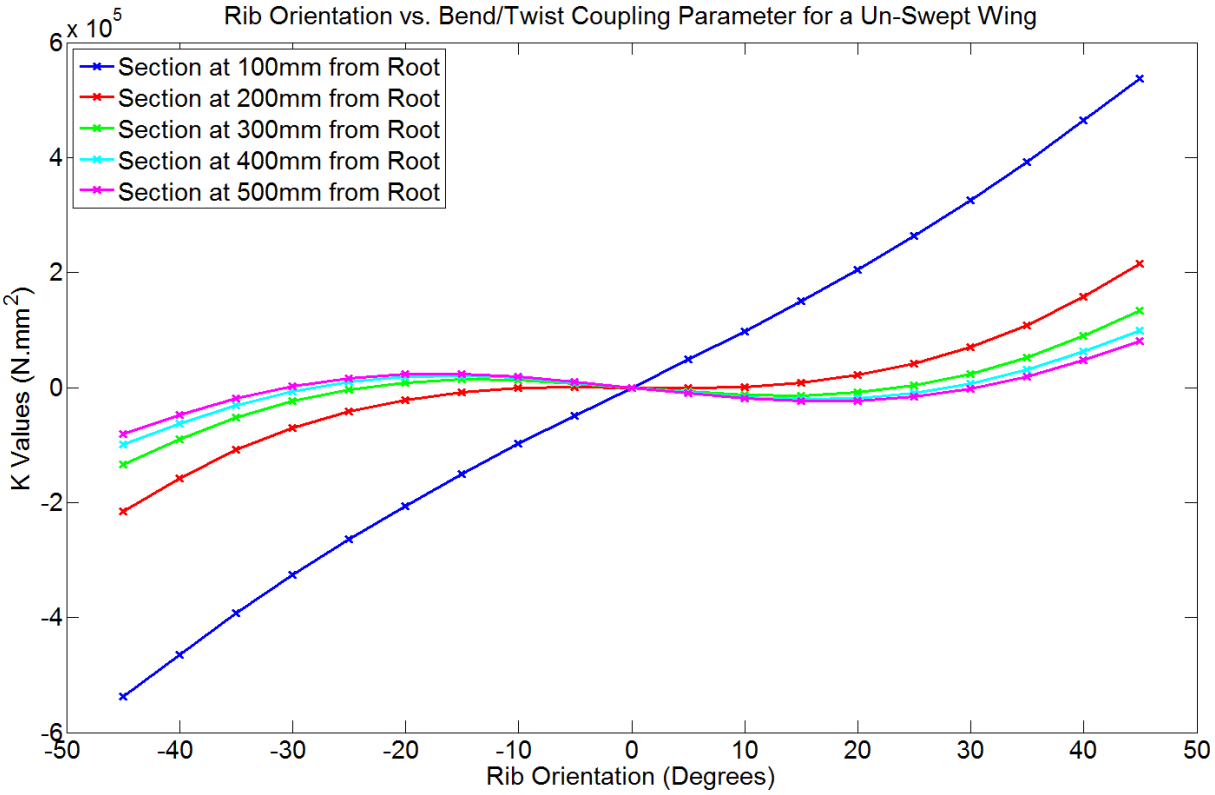

Figure 21. Bend/Twist Coupling Parameter (K) Obtained at Different Sections along the Wing for an Un-Swept Wing with varying Rib Orientation.

Figure 22-23, Figure 24-25 and Figure 26-27 show the wing tip bending stiffness, torsional stiffness and the bend/twist coupling parameter as the wing sweep and the rib orientation change.

Changing the rib orientation and the wing sweep angle with respect to the bending and torsional stiffness creates a saddle surface in both cases. For a given wing sweep angle, the symmetry between bending and torsional stiffness with rib orientation is removed as a wing with a positive sweep angle and a negative rib orientation has a larger bending and torsional stiffness than a wing with a positive sweep angle and a positive rib orientation.

Increasing the wing sweep angle magnitude, in the case of wings with rib orientation at 0^o, reduces both the bending and torsional stiffness of the wing. However, bending and torsional stiffness values are similar for wings with similar structural arrangements. For example, the wing with a sweep angle of -30^o and a rib orientation of -45^o has similar bending and torsional stiffness compared to a wing with sweep angle of 30^o and a rib orientation of 45^o.

The variation of the bend/twist coupling parameter with the wing sweep angle and the rib orientation is a surface principally increasing with the wing sweep angle and respecting the wing sweep angle sign. This means that the primary source of bend/twist coupling is the wing sweep angle.

When considering wings with a rib orientation of 0^o, the surface has three distinct regions: (1) a curved regions from -30^o to -20^o sweep angle, (2) a linear region between -20^o to 20^o sweep angle, (3) finally a curved region from 20^o to 30^o. This means that past a sweep angle of $\pm 20^o$ the relationship between increasing the sweep angle and the bend/twist coupling parameter reduces. When the sweep angle increases from the 0^o angle, the curve relating the bend/twist coupling parameter with the rib orientation changes from a cubic curve with two distinct turning points towards a second order curve. The curve tends to be convex/concave curve for a sweep angle of $-30^o/30^o$.

It should be noticed that some errors exist in the method as the wing with rib orientation and sweep angle of 0^o has a small negative bend/twist coupling parameter ($-10.8 N/mm^2$). As shown in Figure 5, such wing has no tip twist when it bends, hence this value should be zero.

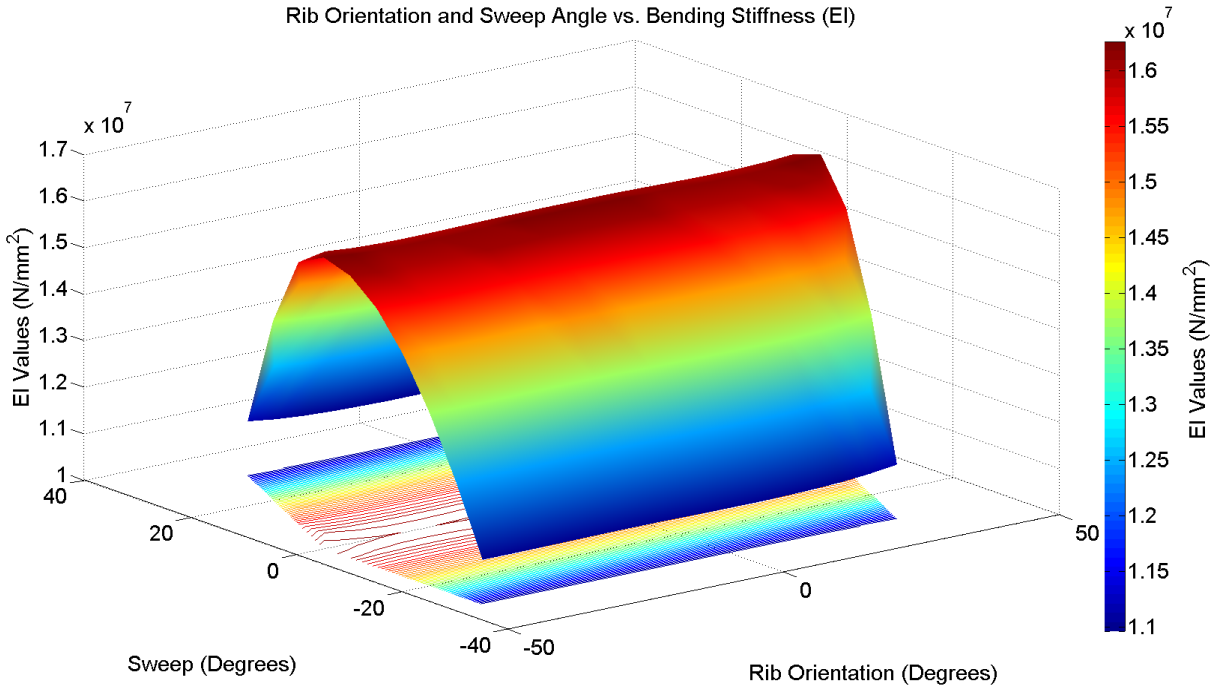

Figure 22. Tip Section Bending Stiffness (EI) Variation with Wing Sweep Angle and Rib Orientation.

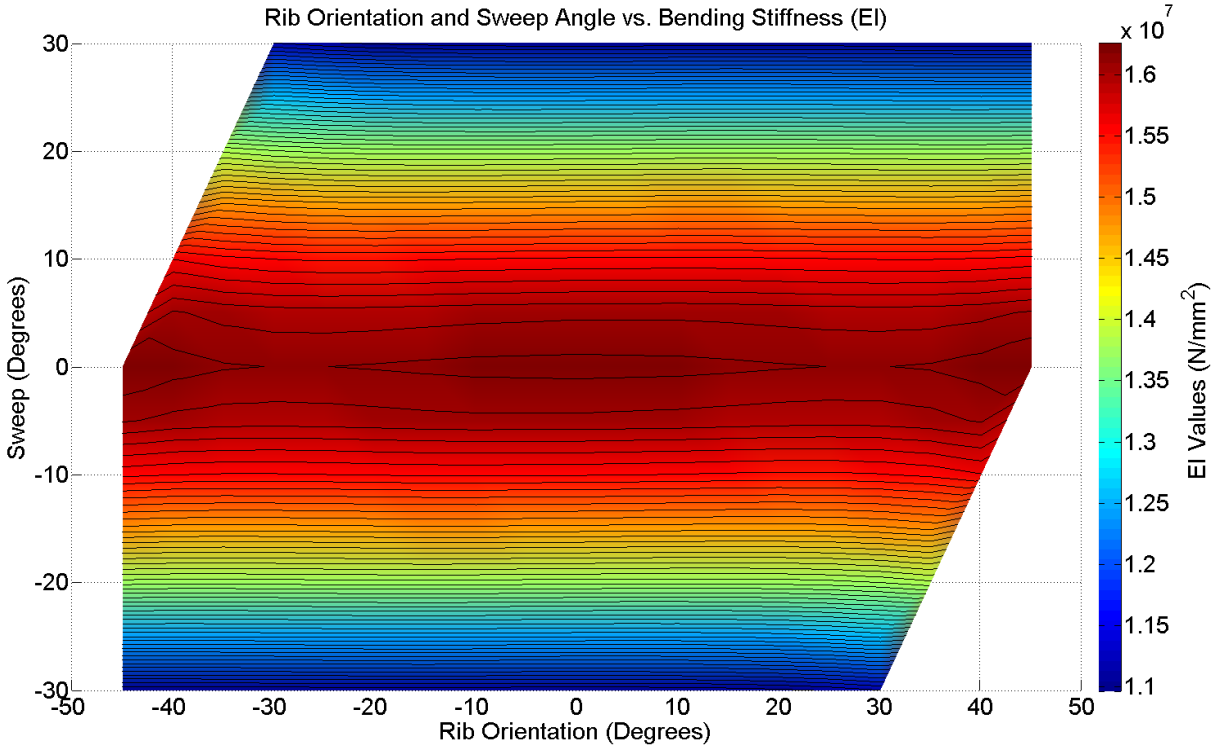

Figure 23. 2D Representation of Variation of the Tip Section Bending Stiffness (EI) with the Wing Sweep Angle and Rib Orientation.

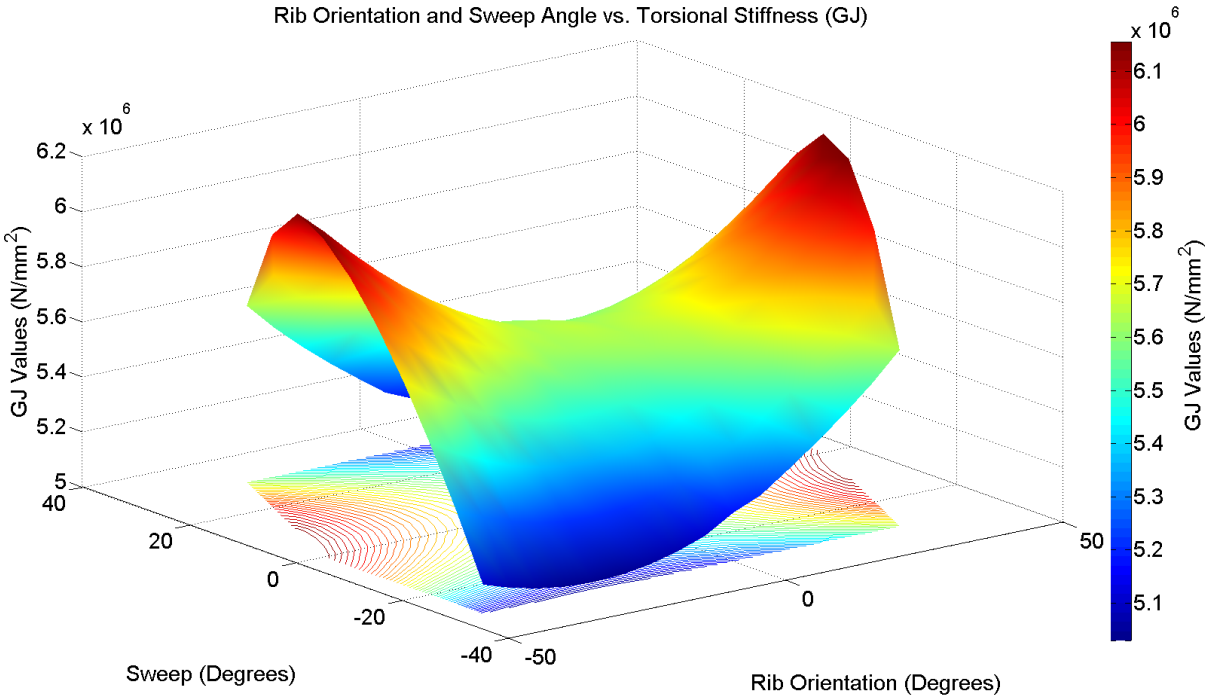

Figure 24. Tip Section Torsional Stiffness (GJ) Variation with Wing Sweep Angle and Rib Orientation.

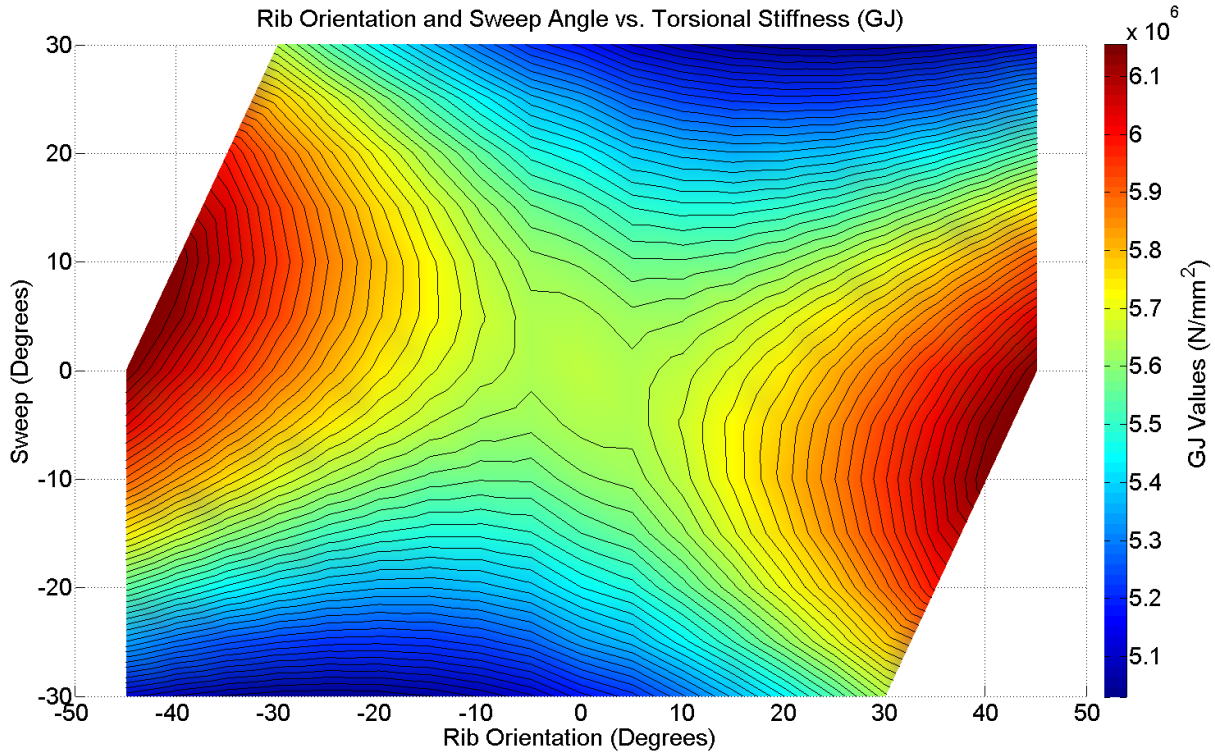

Figure 25. 2D Representation of the Variation of the Tip Section Torsional Stiffness (GJ) with the Wing Sweep Angle and Rib Orientation.

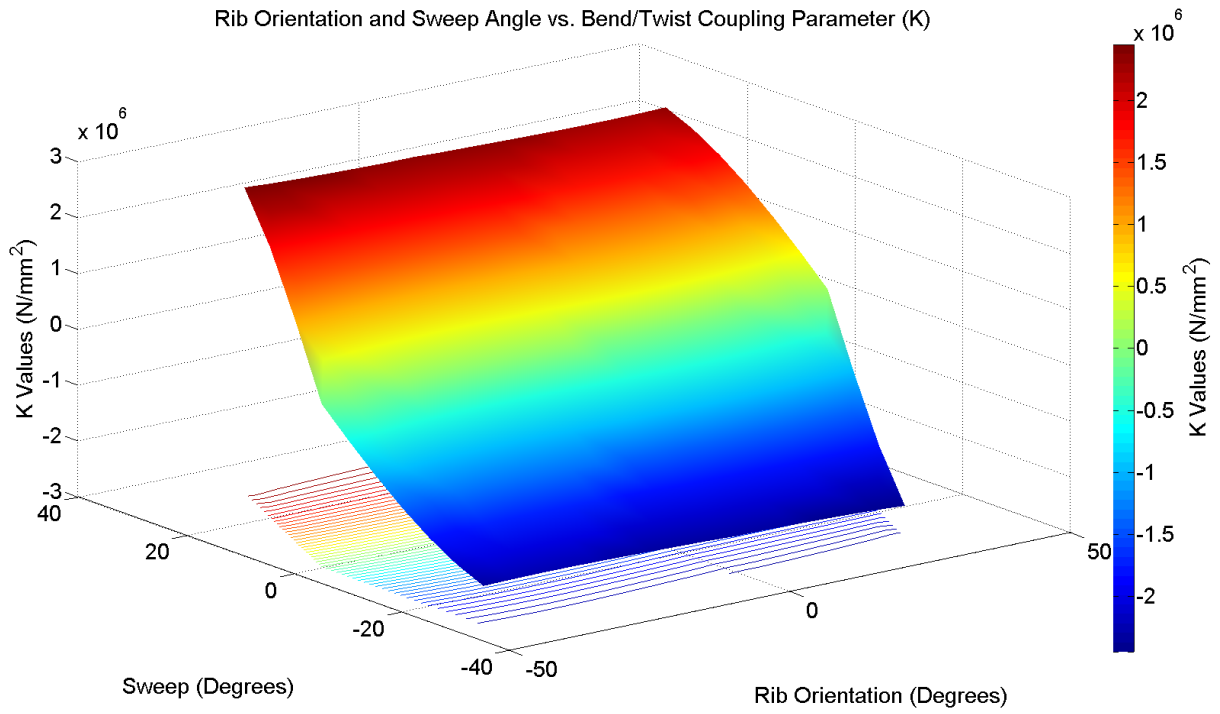

Figure 26. Tip Section Bend/Twist Coupling Parameter (K) Variation with Wing Sweep Angle and Rib Orientation.

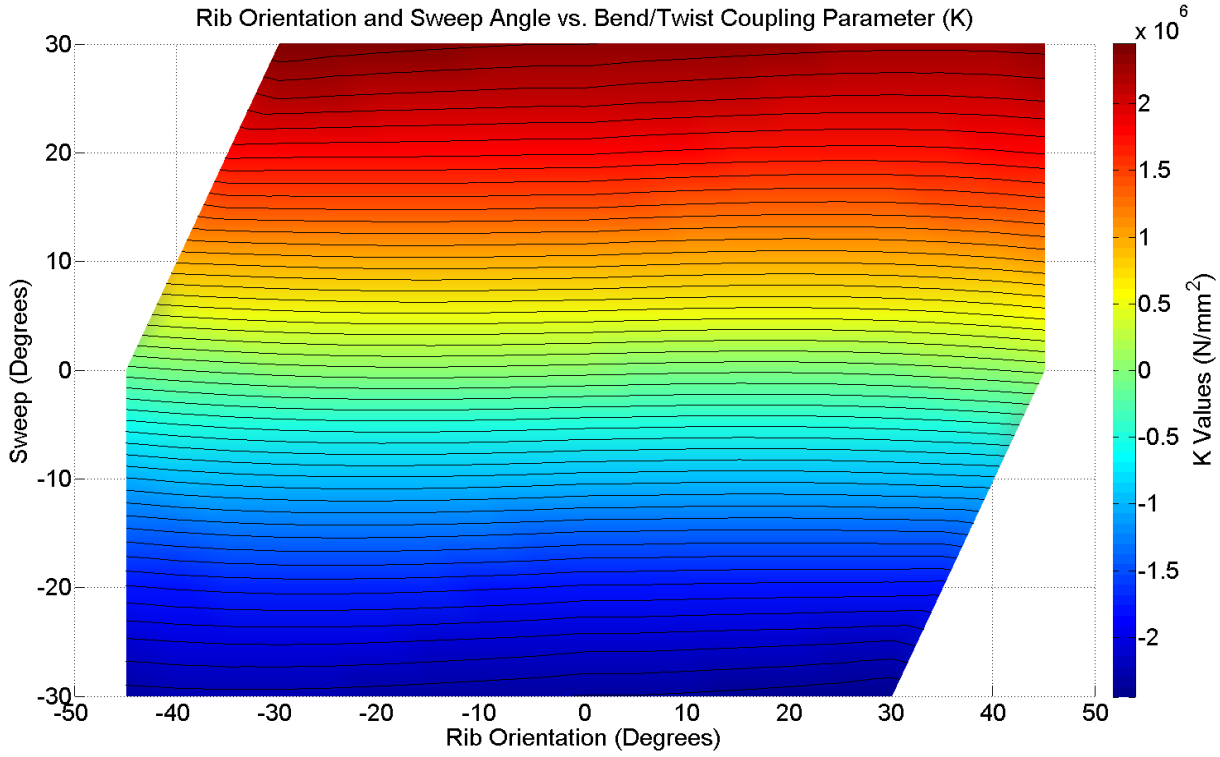

Figure 27. 2D Representation of Variation of the Tip Section Bend/Twist Coupling Parameter (K) with the Wing Sweep Angle and Rib Orientation.

V. Beam Model Results

Having found the beam bending stiffness, torsional stiffness and the bend/twist coupling parameter values for the different wing designs considered, the validity of this data is now tested using a 1D FE beam model and a 1D analytical beam model.

A. 1D Beam Models

The first beam model used is a 1D FE un-swept beam with a length of 500mm split in five sections each of 100mm in length. The model used 1,000 CBEAM elements. The initial beam sectional properties were found using MSC.PATRAN and where inputted in a PBEAM card which defines Euler-Bernoulli beam element properties in terms of the cross-section area, second moment of areas, polar moment of inertia, warping coefficients at both ends of the beam and location of the shear centre with respect to the neutral axis at each end of the beam.

Assuming the warping coefficients are zero and the cross-section of the beam is constant for every wing design considered, the section beam bending and torsional stiffness divided by the material Young's modulus and shear modulus provide us with the bending second moment of area and the polar moment of inertia of each section of every wing concepts. Unfortunately, FE beam models do not allow the use of the bend/twist coupling parameter hence to introduce bend/twist coupling the load application point is moved to half the distance between the tip mid-chord and the tip flexural centre in the opposite direction of the flexural centre. An MPC was used to join the load application point to the tip beam node.

To assess the validity of the bend/twist coupling parameter values found in Section IV an analytical 1D beam model was used. The model was implement in MATLAB and is based on Equation 5 using the sectional properties.

B. Results

The beam models were subjected to a load of 487g similar to the one used in the static analysis in Section III-B. Figure 28 and Figure 29 show the average tip displacement and twist values found by the two beam models considered as well as the 3D FE models. Clearly, both beam models results show similar trends then the 3D FE model results for the variation of the average tip displacement and tip twist as the rib orientation and the wing sweep angle are varied.

At 0^o sweep angle, the 1D FE beam model results have an average difference with the 3D FE model results of -4.3% and 29.4% in tip displacement and twist respectively. The 1D analytical beam model results have an average difference with the 3D FE model results of 0.1% and -39.0% in tip displacement and twist respectively. As the wing sweep angle increases from 0^o the difference in tip displacement values between the different models increases while the difference in twist values between the different models reduces. At 30^o sweep angle, the 1D FE beam model results have an average difference with the 3D FE model results of -16.3% and -14.0% in tip displacement and twist respectively. The 1D analytical beam model results have an average difference with the 3D FE model results of -4.1% and -32.8% in tip displacement and twist respectively.

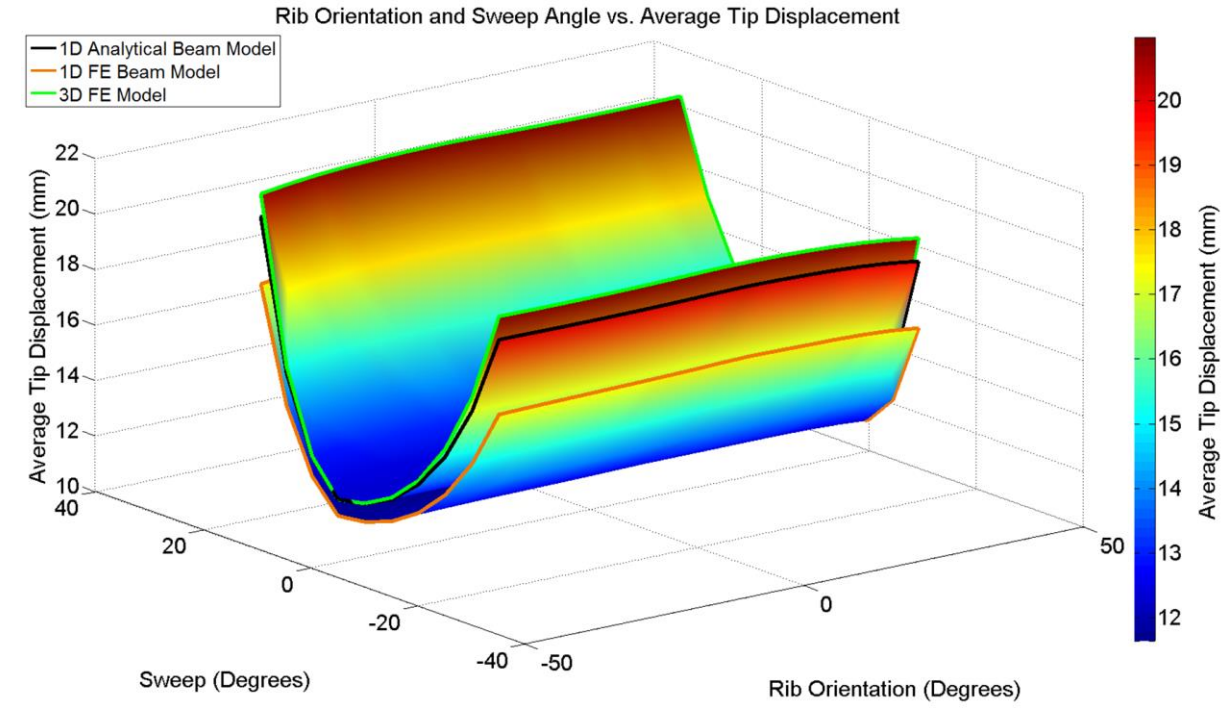

Figure 28. Average Tip Displacement for various Wings with different Rib Orientation and Wing Sweep Angle under Static Load Applied at the Tip Mid-Chord found using 1D FE Beam Model, 1D Analytical Beam Model and 3D FE Model.

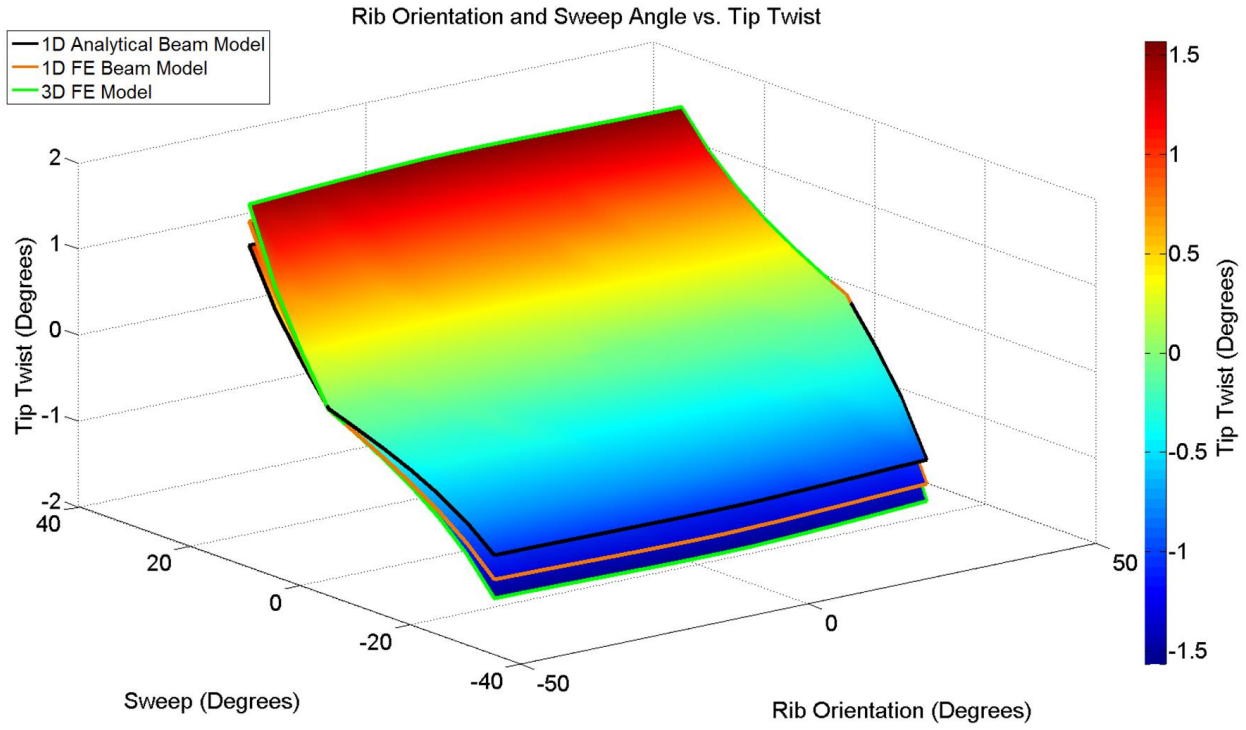

Figure 29. Tip Twist for various Wings with different Rib Orientation and Wing Sweep Angle under Static Load Applied at the Tip Mid-Chord found using 1D FE Beam Model, 1D Analytical Beam Model and 3D FE Model.

VI. Conclusions

In this paper the impact of the wing sweep angle and the rib orientation on the wing's static and dynamic aeroelastic behaviour, natural frequencies, flutter/divergence speed and wing root bending moment during a gust encounter were investigated on un-tapered wings. Overall, the wing sweep angle had a larger impact than the rib orientation at controlling these metrics, e.g. a variation in instability speed and root bending moment during a gust encounter of 92.1% and -37.1% respectively, over a range of $\pm 30^{o}$ sweep, and of 88.0% and -2.2% respectively, over a range of rib orientation of $\pm 30^{o}$. The capability of those two geometric features to change the wing's deformation was characterised by evaluating the equivalent Euler-Bernoulli beam properties (bending stiffness, torsional stiffness and bend/twist coupling parameter) using a series of prescribed loading cases to the 3D FE models. The resulting bend/twist coupling trends due to the wing sweep angle and the rib orientation were observed by equivalent beam section wing models although there are differences towards the root as the beam models do not account for root effects.

Acknowledgments

The author gratefully acknowledges the support of the EPRSC under its ACCIS Doctoral Training Centre grant, EP/G036772/1, the Royal Academy of Engineering and the European Office of Aerospace Research and Development (EOARD). Part of this work was carried out using the computational facilities of the Advanced Computing Research Centre, University of Bristol - http://www.bris.ac.uk/acrc/.

References

1. Airbus.FutureJourneys 2013-2032. (2013). at <http://www.airbus.com/company/market/forecast/?eID=dam_frontend_push&docID=33752>
2. Wright, J. R. & Cooper, J. E. *Introduction to Aircraft Aeroelasticity and Loads*. (Wiley, 2007).
3. Shirk, M. H., Hertz, T. J. & Weisshaar, T. A. Aeroelastic tailoring-theory, practice, and promise. *Journal of Aircraft* **23,** 6–18 (1986).
4. Weisshaar, T. A. Aeroelastic tailoring of forward swept composite wings. *Journal of Aircraft* (1981).
5. Weisshaar, T. A. Aeroelastic tailoring - Creative uses of unusual materials. *AIAA/ASME/ASCE/AHS 28th Structures, Structural Dynamics and Materials Conference, 6-8 April, Monterey, California, U.S.A.* (1987).
6. Kim, T. & Hwang, I. H. Optimal design of composite wing subjected to gust loads. *Computers & Structures* **83,** 1546–1554 (2005).
7. Guo, S. Aeroelastic optimization of an aerobatic aircraft wing structure. *Aerospace Science and Technology* **11,** 396–404 (2007).
8. Manan, A., Vio, G. A., Harmin, M. Y. & Cooper, J. E. Optimization of aeroelastic composite structures using evolutionary algorithms. *Engineering Optimization* **42,** 171–184 (2010).
9. Stodieck, O., Cooper, J. E., Weaver, P. M. & Kealy, P. Improved aeroelastic tailoring using tow-steered composites. *Composite Structures* **106,** 703–715 (2013).
10. Maute, K. & Allen, M. Conceptual design of aeroelastic structures by topology optimization. *Structural and Multidisciplinary Optimization* **27,** 27–42 (2004).
11. Kolonay, R. M. & Kobayashi, M. H. Topology, Shape, and Sizing Optimization of Aircraft Lifting Surfaces Using a Cellular Division Method. *13th AIAA/ISSMO Multidisciplinary Analysis Optimization Conference, Forth Worth, Texas, U.S.A* (2010).
12. Locatelli, D., Mulani, S. B. & Kapania, R. K. Wing-Box Weight Optimization Using Curvilinear Spars and Ribs (SpaRibs). *Journal of Aircraft* **48,** 1671–1684 (2011).
13. Vio, G. A., Georgiou, G. & Cooper, J. E. Design of Composite Structures to Improve the Aeroelastic Performance. *53rd AIAA/ASME/ASCE/AHS/ASC Structures, Structural Dynamics and Materials Conference, 23-26 April 2012, Honolulu, Hawai, U.S.A* (2012).
14. Vio, G. A. & Fitzpatrick, I. R. Design of Composite Structures for Improved Aeroelastic Performance. *28th ICAS, 23-28 September 2012, Brisbane, Australia* (2012).
15. Brampton, C. J., Kim, H. A. & Cunningham, J. L. Level Set Topology Optimisation of Aircraft Wing Considering Aerostructural Interaction. *12th AIAA Aviation Technology, Integration, and operations (ATIO) Conference and 14th AIAA/ISSM 17-19 September 2012, Indianapolis, Indiana, U.S.A* (2012).
16. Jutte, C. V., Stanford, B. K., Wieseman, C. D. & Moore, J. B. Aeroelastic Tailoring of the NASA Common Research Model via Novel Material and Structural Configurations. *53th AIAA/ASMe/ASCE/AHS/SC Structures, Structural Dynamics, and Material Conference, National Harbor, Maryland, U.S.A.* (2014).
17. Dunning, P. D., Stanford, B. K. & Kim, H. A. Aerostructural Level Set Topology Optimization for a

Common Research Model Wing. *10th AIAA Multidisciplinary Design Optimization Conference, 13-17 January 2014, National Harbor, Maryland, U.S.A.* (2014).
18. Liu, Q., Mulani, S. & Kapania, R. K. Global / Local Multidisciplinary Design Optimization of Subsonic Wing. *53th AIAA/ASMe/ASCE/AHS/SC Structures, Structural Dynamics, and Material Conference, National Harbor, Maryland, U.S.A.* (2014).
19. Francois, G. & Cooper, J. E. Novel Structural Wing Designs for Forward Swept Wings. *2014 Royal Aeronautical Society Biennial Applied Aerodynamics Research Conference, 22-24 July 2014, Bristol ,U.K.* (2014).
20. Francois, G., Cooper, J. E. & Weaver, P. M. Aeroelastic Tailoring of Composite Wings using Internal Structural Members Shape and Stacking Sequence. *4th Aircraft Structural Design Conference, 7-9 October 2014, Belfast, U.K.* (2014).
21. Dunning, P. D., Stanford, B. K. & Kim, H. A. Level - Set Topology Optimization with Aeroelastic Constraints. *56th AIAA/ASMe/ASCE/AHS/SC Structures, Structural Dynamics, and Material Conference, Kissimmee, Florida, U.S.A.* (2015).
22. Liu, Q., Jrad, M., Mulani, S. B. & Kapania, R. K. Integrated Global Wing and Local Panel Optimization of Aircraft Wing. *56th AIAA/ASMe/ASCE/AHS/SC Structures, Structural Dynamics, and Material Conference, Kissimmee, Florida, U.S.A.* (2015).
23. Stanford, B. K., Wieseman, C. D. & Jutte, C. V. Aeroelastic Tailoring of Transport Wings Including Transonic Flutter Constraints. *56th AIAA/ASMe/ASCE/AHS/SC Structures, Structural Dynamics, and Material Conference, Kissimmee, Florida, U.S.A.* (2015).
24. Harmin, M. Y., Ahmed, A. T. & Cooper, J. E. Aeroelastic Tailoring of Metallic Wing Structures. *52nd AIAA/ASME/ASCE/AHS/ASC Structures, Structural Dynamics and Materials Conference, 4-7 April 2011, Denver, Colorado, U.S.A* (2011).
25. Francois, G., Cooper, J. E. & Weaver, P. M. Aeroelastic Tailoring using Rib / Spar Orientations : Experimental Investigation. *56th AIAA/ASMe/ASCE/AHS/SC Structures, Structural Dynamics, and Material Conference, Kissimmee, Florida, U.S.A* (2015).
26. Francois, G., Cooper, J. E. & Weaver, P. M. Aeroelastic Tailoring Using Crenelated Skins – Modelling and Experiment. in *International Forum on Aeroelasticity and Structural Dynamics, June 28 - July 2, Saint Petersburg, Russia (2015*).
27. Tatham, R. Shear Centre, Flexural Centre and Flexural Axis: An Attempt to Clear up Current Confusion and Provide Definitions Differentiating Between the Three Terms. *Aircraft Engineering and Aerospace Technology* **23,** 209–210 (1951).
28. Stodieck, O., Cooper, J. E. & Weaver, P. M. On the Interpretation of Bending-Torsion Coupling for Swept, Non-Homogenous Wings. *56th AIAA/ASMe/ASCE/AHS/SC Structures, Structural Dynamics, and Material Conference, Kissimmee, Florida, U.S.A.* (2015).
29. Rodden, W. P. & Johnson, E. H. *MSC/NASTRAN Aeroelastic Analysis User's Guide v68*. (The MacNeal-Schwendler Corporation, 1994).
30. Johnson, E. H. MSC Developments in Aeroelasticity. in *1997 MSC Aerospace Users' Conference* 1–9 (1997).
31. European Aviation Safety Agency. *Certification Specifications for Normal, Utility, Aerobatic, and Commuter Catergory Aeroplanes CS 23*. (2013).